University of Louisville

ThinkIR: The University of Louisville's Institutional Repository

Electronic Theses and Dissertations

5-2019

Capture and Release Gels for Optimized Storage (CaRGOS)

Theodore S. Kalbfleisch II
University of Louisville

Capture and Release Gels for Optimized Storage [CaRGOS]

By

Theodore Kalbfleisch II
B.S. Chemical Engineering, University of Louisville, Fall 2017

A Thesis
Submitted to the Faculty of the
University of Louisville
J.B. Speed School of Engineering
as Partial Fulfillment of the Requirements
for the Professional Degree

MASTER OF ENGINEERING

Department of Chemical Engineering

May 2019

CAPTURE AND RELEASE GELS FOR OPTIMIZED STORAGE (CARGOS)

Submitted by: _Ted Kalbfleisch_

Theodore Kalbfleisch II

A Thesis Approved On

May 22, 2019

Date

by the Following Reading and Examination Committee

Dr. Gautam Gupta, Thesis Director

Dr. Robert Keynton, Committee Member

Dr. Vance Jaeger, Committee Member

ACKNOWLEDGMENTS

ABSTRACT

Unassisted, the lifetime of many proteins outside their natural environment is very short. Scientists generally need to extract the sample, often in remote locations, and then transport, isolate, and store such biospecimens relatively far from the point of origin in order to study them. Currently, the most commonly used methods for storage of biospecimens are cryopreservation or refrigeration which, though effective, have their fair share of flaws. Cryopreservation and refrigeration-based storage of biospecimens requires a great deal of space and other resources to be effective. Furthermore, the hardware required for cold storage does not transport well. These factors make such storage methods impractical for use in the field and even some laboratories[1-3]. Due to repeated strain on biomolecules from crystallization, rapid degradation occurs after repeated freezing and thawing; this problem could be avoided by storing specimens at ambient temperatures. Herein, we report a novel method for long-term room-temperature aqueous biomolecule storage utilizing rapidly fabricated silica sol-gel networks. By adjusting solution conditions such as acidity, salinity, buffer concentration, and silica density, it is possible to tailor sol-gel chemistry to create hospitable silica structures to support a variety of biomolecules. We have demonstrated the preservation of RNA and Hemoglobin samples for up to 28 days and 31 days respectively, under ambient

conditions, using this technique. Upon coupling the amenability of the sol-gel structure with a contemporary rapid synthesis method, silica sol-gels become *Capture and Release Gels for Optimized Storage* (*CaRGOS*).

TABLE OF CONTENTS

LIST OF TABLES

LIST OF FIGURES

I. INTRODUCTION

Biomolecules are difficult to store but important for human health studies and molecular biology research. Their complex chemistry lends itself to aid in finely tuned processes, however when taken out of their natural environment the same complex chemistry makes them unstable.

The proneness to degradation of these materials make it very difficult to preserve samples between studies and establish standard operating procedures between institutions. For example, two institutions working on the exact same material may get different results owing to the varying states of degradation between the two samples caused by differences in transportation, handling, etc. These issues lead to inconsistencies between studies conducted at separate facilities and could cast doubt on independently-reported conclusions [4]. In order to further standardize the study of biospecimens, efforts must be made to combat their natural fragility. To this end, efforts have been made to stabilize biospecimens for transport and study.

Cryopreservation under liquid nitrogen is a well-established method for indefinite storage of unstable biomolecules, but it requires a great deal of infrastructure, safeguards, and maintenance[5]. While there are commercial biobanks which can indefinitely store large numbers of individual samples cryogenically and distribute them when needed, this process becomes expensive, time-consuming, and logistically difficult for less well-equipped facilities. Additionally, to study the samples, they must be removed from cold storage and thawed [4, 6]. Johnny C. Akers et al observed that repeatedly thawing and freezing samples for study and storage decreases the integrity incrementally with each

1

cycle, making the prospect of using cold storage to extensively research one specimen risky [4, 7].

Room temperature preservation of biomolecules has been sought after in order to cut down on the resources required for cryopreservation. Commercial products exist to store biomolecules at room temperature, but these products generally utilize ultra-dry conditions [6, 8]. Accessing and storing samples with these products requires multiple rehydration and dehydration steps which incrementally degrade the sample [5].

Based on the strengths and flaws of cryopreservation, ultra-dry storage, and traditional sol-gels, an ideal technique for encapsulation and preservation of biomolecules should be:

- Done in an aqueous medium which is as inert as possible

- Repeatable in any given location

- Easy enough to carry out with basic instruction

- Sterile [9-11]

The biomolecule should be prepared for long-term storage at ambient temperatures, protected from protease and nuclease, and be easily recoverable (34). Current technologies are unable to fulfill all these requirements.

Providing all institutions, individuals, and facilities in need of long-term robust storage of various biomolecules a means to do so quickly, easily, and at ambient conditions can be achieved through *Capture and Release Gels for Optimized Storage (CaRGOS)*. With very little manufacturing time and cost, *CaRGOS* sol-gel technology preserves biomolecules and biospecimens for storage and transport at ambient to above-ambient temperatures. Sample storage and recovery is possible for anyone with access to

the requisite reagent chemicals and a microwave. The technique provides continuous access to the sample without time-consuming and damaging thawing or rehydration steps. *CaRGOS* would facilitate processing of biospecimens collected in remote areas by enabling transportation to analytical facilities without specialized accommodations such as cryopreservation equipment. The adoption of *CaRGOS* will not only circumvent the resource consumption required to consistently operate cold storage devices but will also improve the integrity of the biomolecules during experiments at ambient temperatures.

The following text shall present a new and novel method of biomolecule preservation which not only satisfies the necessary criteria to be useful but also goes above and beyond previous technologies. Through careful modification of solution chemistry and use of a standard microwave oven, silica sol-gel becomes the powerful *Capture and Release Gel for Optimized Storage* (*CaRGOS*). In order to characterize the performance of *CaRGOS,* microRNA 21 and Hemoglobin have been encapsulated in *CaRGOS* for extended periods, and their integrity assessed at several time intervals before successful recovery of the specimens.

SOL – GEL CHEMISTRY

OVERVIEW

Sol-gel techniques have been looked towards as a possible solution for biomolecule storage since the 1930s [12]. Due to their optical clarity and porous nature, immobilizing a protein within a sol-gel network allows for study and application of the molecule's native structure and function without exposure to potentially harmful conditions [13, 14]. Sol-gels are colloidal suspensions that exist as a collection of particles that agglomerate or form complex branching network that ultimately forms the gel [12]. Through the sol-gel method, researchers have been able to explore unique formulations of biocompatible ceramics to function as support materials, implants, drug delivery, and stimulants for certain biological cell responses[14, 15]. The physical characteristics of the sol-gel such as particle size, network geometry, porosity, and surface potential can be altered during or post-synthesis with relative ease to assist in the study of biomaterials[16].

The use of silica sol-gels has received special attention, as it is a relatively simple aqueous process with tunable salinity and thus is inherently biocompatible [17, 18]. Though silica sol-gels show great promise, the most common preparation methods do not lend themselves well toward widespread adoption. Traditionally, silica sol-gels implement alcohols as co-solvents, contain acidic or basic catalysts, or utilize complex formulations which do not scale well. The co-solvents and catalysts are potentially harmful to biospecimens if they are present in the final gel [19-26].

By employing microwave hydrolysis, biocompatible sol-gels can be synthesized at a faster rate than ever before without employing co-solvents or acidic/basic catalysts. Relatively low TMOS precursor concentration formulations have been fully hydrolyzed

within 30 seconds of microwave exposure and the resulting sol-gels have shown promise

as biomaterial storage materials.

II. INSTRUMENTATION AND EQUIPMENT

A. Infrastructure and Equipment

Fume hood

Microwave 1200 Watt with viewing window in order to monitor samples during use.

Vortex machine

Dynamic Light Scattering (DLS) machine

Fourier Transform Infrared spectrophotometer

UV-Vis spectrophotometer

Reva Educational Raman platform.

Micropipettes capable of measuring as little as 0.5 uL

Sealable glass vessel with 2-3 ventilation holes in the cap for gasified methanol

B. Chemicals

Tetramethyl orthosilicate 99% (TMOS) from Acros Organics.

Tris-EDTA (TE) buffer from Sigma Aldrich.

Sodium Chloride (NaCl) from Sigma Aldrich.

Polymethylmethacrylate UV-grade cuvettes from VWR.

III. Procedure

A. TMOS Microwave Hydrolysis.

To prepare the sol-gel, TMOS and NFW were combined in the desired v/v %

concentration in a clear glass vial capped with a modified top to vent. The mixture was

agitated with a Vortex mixer to uniformly disperse the components. The vented container

was placed in a 1200-watt microwave and microwaved at full power for 15-30 seconds or

until boiling. If the mixture began boiling prematurely, it was removed, mixed, and

allowed to settle for a few seconds before completing the microwave process. The

microwaves served to hydrolyze TMOS, forming silicic acid and methanol. Both

products of this reaction are miscible in water, so if any distinct TMOS bubbles were still

observed within the mixture, the process was repeated until an optically clear

homogenous liquid was achieved. The mixture was allowed to sit uncovered in a fume

hood and off-gas the bulk of the gaseous methanol before proceeding.

B. UV-Vis Spectroscopy

The utility of sol-gels as a storage medium while also allowing spectral analysis

without total removal of the sample was explored. UV-vis spectroscopy was performed

on a set of four sol-gels of concentrations 0.5, 1.0, 5.0, and 10.0% v/v after hydrolysis

and at periods of 1, 4, 7, 10, and 14 days under ambient room conditions. An Agilent

Cary win 60 UV-Vis, at a range of 280 – 1000 nm, collecting data every 1 nm, with an

average time of 0.1 second, and a scan rate of 600 nm/minute. The resulting spectra

illustrate the ability of a sol-gel network to allow for reliable and accurate analysis of

stored materials at different network densities as they continue to form.

C. Raman Spectroscopy

Raman spectra was collected for TMOS/H_2O before and after microwave hydrolysis as well as *CaRGOS* samples using a Reva Educational Raman platform. The laser power of 450.0 mW and current 959.0 mA was optimized to analyze vibrational and rotational motions of silica (Si-O) bonds. The laser temperatures [diode = 30 °C; Case = 24.4 °C] and spectrometer temperature [23.1 °C] were optimized for collecting Raman spectra.

D. Fourier Transform Infrared Spectroscopy (FTIR)

FTIR was performed using a PerkinElmer Spectrum 100 FT-IR Spectrophotometer. Each measurement was taken between 550 and 2500 cm^{-1}, 8 scans per measurement, and corrected using baseline and attenuated total reflection correction.

E. Dynamic Light Scattering (DLS)

A NanoBrook Zeta PALS from Brookhaven Instruments was used to collect DLS and zeta potential measurements. Three scans consisting of 20 cycles were performed and averaged were used to form the results presented.

F. Zeta Potential Measurements

Using the NanoBrook Zeta PALS from Brookhaven Instruments, zeta potential measurements were collected using 80 Hz frequency. Two continuous measurements totaling in 4 minute collection time were used to form the results of each dataset presented.

IV. Results and Discussion of Results

A. Optics.

Silica sol-gels have been explored as biomolecule storage methods in the past due to their optical clarity and biocompatibility [9, 27-29]. In order to assess the possibility of sample analysis while in *CaRGOS* over extended periods, the optical clarity of gels was assessed via UV-vis analysis at several points in time with 0.5, 1.0, 5.0, and 10.0 % v/v. At times of 1, 4, and 7 days after hydrolysis as well as immediately after hydrolysis three spectra were collected between 280 – 1000 nm and averaged for each formulation, Figure 1.
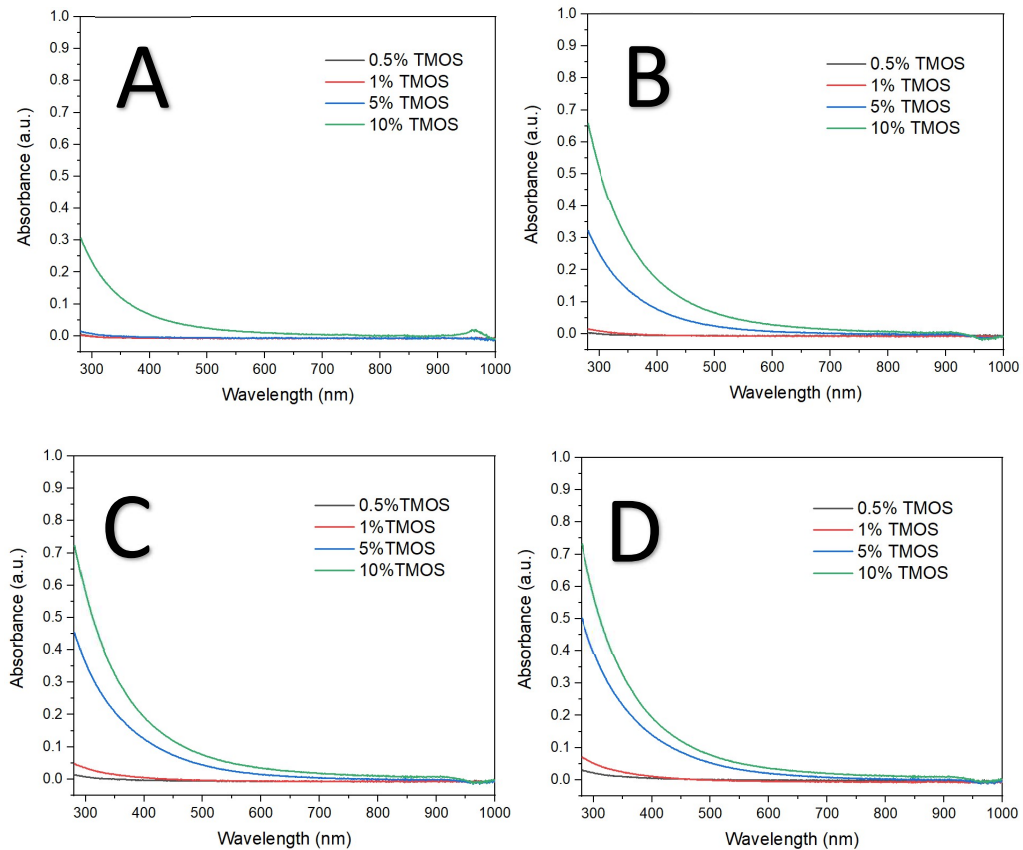
FIGURE 1 – UV-Vis Spectra of TMOS Formulations at 0 Days (A) 1 Day (B) 4 Days (C) and 1 Week (D)

In the lower, more aqueous concentrations (0.5 & 1.0 % v/v), there is little to no change in the bulk of the spectra, and an > 0.1 change in absorbance at lower wavelengths after one week. At 5 % v/v TMOS concentration, no significant change in the spectra was observed initially before any gelation was observed, but over the course of one day after gel formation the absorbance rose significantly. 10 % v/v TMOS formed a gel within minutes of hydrolysis and resulted in fairly significant increase in absorbance at lower wavelengths (280 – 600 nm). After one day, each formulation gradually increases in absorbance at a decreasing rate. This trend, along with the absence of any particular peaks suggests that the absorbance is increasing due to light scattering by a more ordered silica network and suspended nanoparticles [30]. Network formation in silica sol-gels continues until the gel is completely dried of water, so it is reasonable why a more aqueous formulation results in higher optical stability over longer periods of time [31-33]. Though an overall increase in absorbance was observed in solid gel samples, no specific peaks formed across the spectra, so characterization of samples within the gel matrix over time is still possible to some extent.

B. Hydrolysis Efficiency

The hydrolysis of TMOS precursor molecules occurs in four steps:

(Equation 1) $$Si(OCH_3)_4 + H_2O \leftrightarrow Si(OCH_3)_3(OH) + CH_3OH$$

(Equation 2) $$Si(OCH_3)_3(OH) + H_2O \leftrightarrow Si(OCH_3)_2(OH)_2 + CH_3OH$$

(Equation 3) $$Si(OCH_3)_2(OH)_2 + H_2O \leftrightarrow Si(OCH_3)_1(OH)_3 + CH_3OH$$

(Equation 4) $$Si(OCH_3)(OH)_3 + H_2O \leftrightarrow Si(OH)_4 + CH_3OH$$
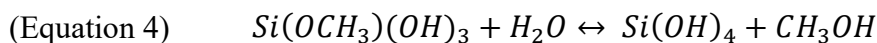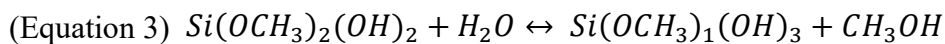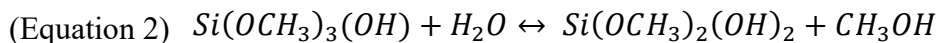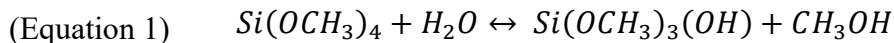
Due to the immiscible nature of TMOS and water, contact between these two reagents can be a limiting factor. Traditionally, organic co-solvents such as alcohols are used to homogenize the mixture in order to increase reagent interaction [33, 34]. While this is ultimately beneficial to the hydrolysis rate, the presence of excess alcohols in *CaRGOS* is detrimental to its application in long term, stable biomolecule storage. Because the hydrolysis of TMOS inherently produces substantial amounts of methanol it is reasonable to assume that rapid hydrolysis of an immiscible mixture would provide enough methanol to assist in the dissolution and hydrolysis of the initial precursor, while also minimizing alcohol concentration in the final product.

To the end of achieving a more rapid hydrolysis of precursor molecules acids and bases are generally used as catalysts. Acidic catalysis adds a protonation fast step that makes TMOS more susceptible to backside attack by water, while nucleophilic hydroxyl groups readily attack the silicon atoms in alkaline catalysis [35]. Though effective, extreme acidic and basic conditions can result in denaturation or degradation of biological molecules making the use of such catalysts difficult for sol-gel use in biomolecule storage without further processing, undermining the convenience of rapid hydrolysis.

Using the techniques stated above, research has been done on sol-gel synthesis under a variety of conditions in order to optimize hydrolysis and condensation in order to achieve a wide range of structures with an even wider range of properties, but in most cases great amounts of heat and time are still required.

In order to rapidly hydrolyze TMOS without the use of organic co-solvents or acidic/alkaline catalysis, a standard microwave can instead be used. By agitating the

TMOS/Water mixture and quickly subjecting it to 30 seconds of microwave exposure a homogenous mixture is rapidly achieved, Figure 2.
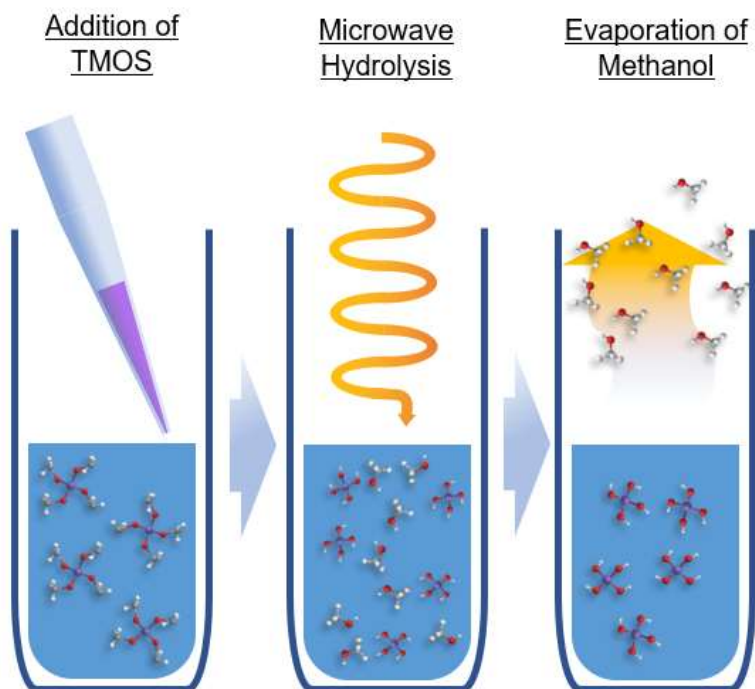
FIGURE 2 – TMOS Microwave Hydrolysis

Agitation by vortexing the mixture serves to disperse TMOS precursor throughout the water in small droplets in order to maximize the contact of reagents without use of co-solvents. If left unreacted for too long the dispersed TMOS will once again aggregate and reduce total surface contact.

Condensation of silica networks can occur in two ways, the hydroxyl group of one precursor replaces another hydroxyl group creating an SiO_2 bond and H_2O, or by replacing an alkoxy group from a not yet fully hydrolyzed precursor molecule creating an SiO_2 bond and CH_3OH as seen in Equations 5 & 6.

<div align="center">Water Condensation</div>

(Equation 5) $\equiv SiOH+ \equiv SiOH \leftrightarrow \equiv Si - O - Si \equiv +OH_2$

<div align="center">Methanol Condensation</div>

(Equation 6) $\equiv SiOH+ \equiv SiOCH \leftrightarrow \equiv Si - O - Si \equiv +CH_3OH$
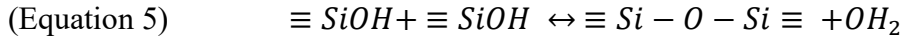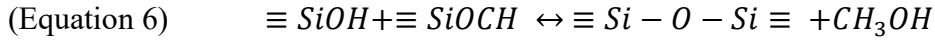
Stoichiometrically, there should be 4X higher methanol produced during hydrolysis of TMOS than the initial TMOS concentration. Due to the nature of this hydrolysis method, the solution will be subjected to high temperatures and evaporation of the bulk of methanol produced is inevitable, but a more complete hydrolysis of TMOS at any concentration would still ultimately result in higher ratio of methanol produced to initial precursor used.

To quantify the effectiveness of the microwave hydrolysis of TMOS at different precursor concentrations, mixtures of varying TMOS content (0.5, 1, 5, 10 % v/v) were hydrolyzed in a microwave for 30 seconds and the methanol content soon after hydrolysis was measured using raman spectroscopy and a calibration curve of methanol peak intensity at the 1033 cm^{-1} characteristic peak [36] (Figure 17 in APPENDIX I). Figure 3 shows the resulting spectra before and after hydrolysis of each TMOS content.
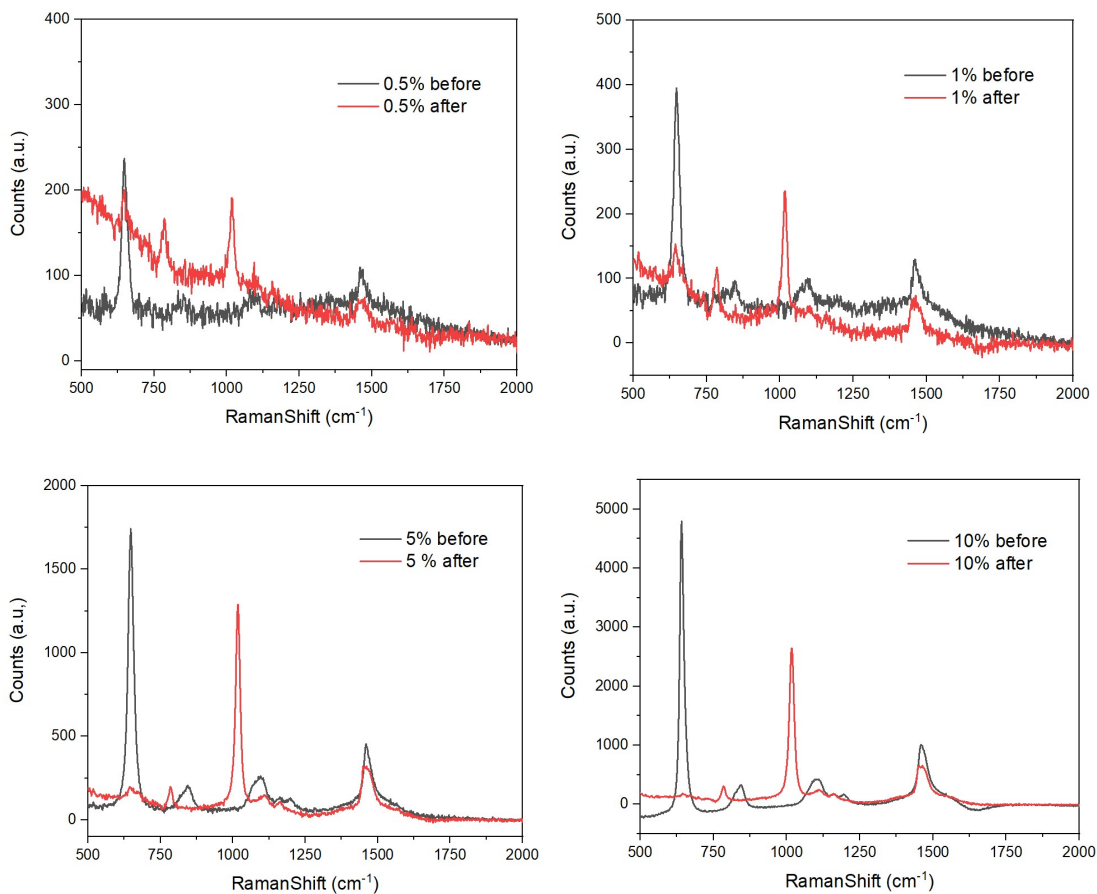
FIGURE 3 – Raman Spectra of 0.5 – 10 % v/v TMOS Formulations

The calculated methanol concentrations after 30 second microwave hydrolysis are displayed in TABLE I below.

TABLE I

METHANOL CONTENT OF HYDROLYZED TMOS FORMULATIONS

Sample	Methanol Peak (Counts)	Methanol Content (% v/v)
0.5 % v/v TMOS	191.0	0.7356
1.0 % v/v TMOS	235.3	0.9104
5.0 % v/v TMOS	1288.2	5.0645
10 % v/v TMOS	2640.4	10.3995

Theoretically, the molar methanol concentration should be four times that of initial TMOS precursor. The calculated theoretical methanol concentration of fully hydrolyzed 10 mL samples is in TABLE II below.

TABLE II

THEORETICAL AND CALCULATED MOLAR METHANOL YIELD

v/v % TMOS	0.5	1.0	5.0	10.0
Theoretical Methanol (mol/L)	0.1353	0.2707	1.3533	2.7066
Calculated Methanol (mol/L)	0.1331*	0.2250	1.2519	2.5707
Hydrolysis Efficiency (%)	98.4	83.1	92.5	95.0
* Value calculated from curve exceeded theoretical. Regression from other calculated values was used				

The results obtained indicate near total hydrolysis of all TMOS precursor after only 30 seconds of exposure to microwaves assuming no methanol evaporated before or during the measurements.

C. Condensation.

1. FTIR Analysis.

With the hydrolysis of TMOS precursor characterized, it is imperative to the application of sol-gels for biomolecule storage that condensation of the sol occurs in order to form a silica structure. It is clear in the higher precursor formulations (5, 10 % v/v) that silica networks were forming because they produced solid gels within 24 hours of hydrolysis, but in the lower concentrations (0.5, 1 % v/v) no visible networks were formed within the sol and remained aqueous. Infrared spectroscopy has been extensively

utilized to explore the structural characteristics of bioactive silicas fabricated through the sol-gel method [37-39]. FTIR was utilized to confirm the formation of silica structures in all four formulations of *CaRGOS* after 1 day of settling, Figure 4.
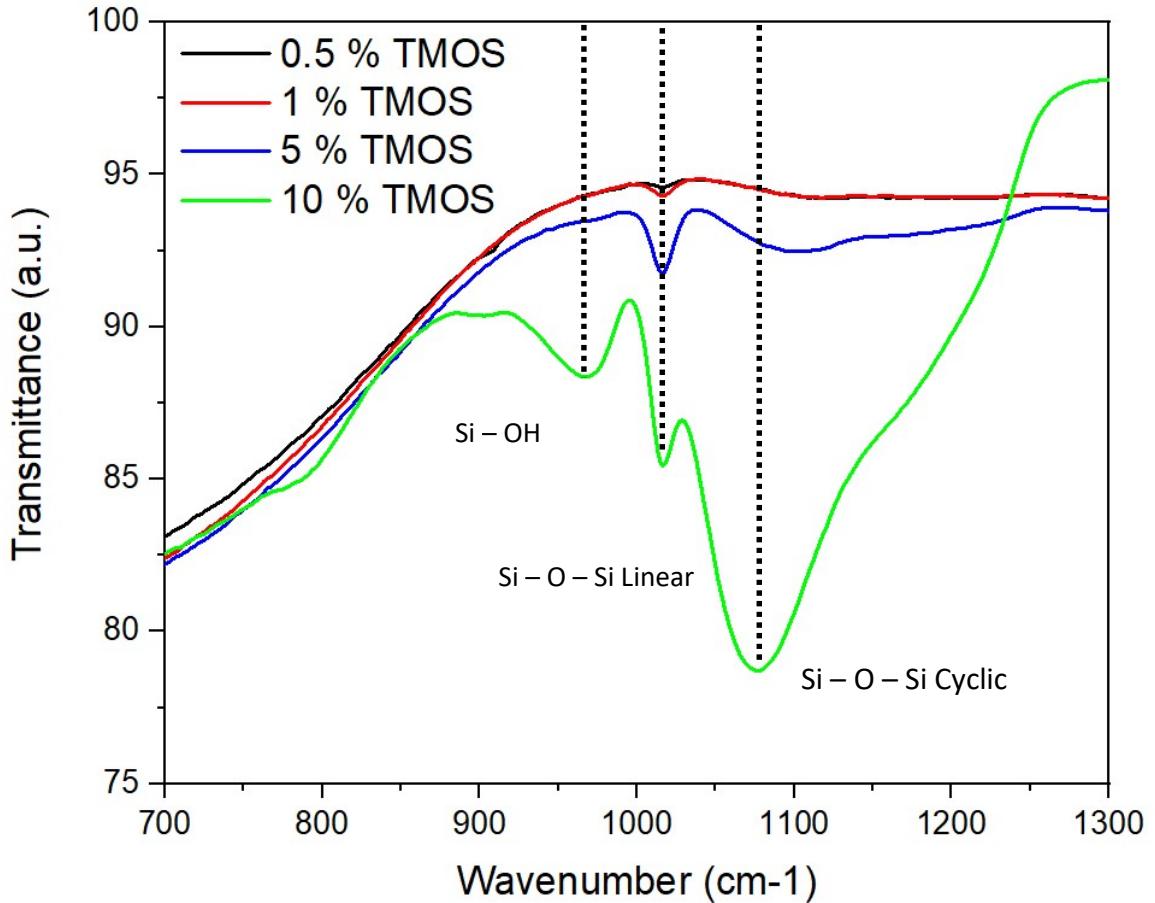
FIGURE 4 – FTIR of Sol-gel Solutions 1 Day After Hydrolysis

The characteristic region used to identify Si – O – Si vibrational mode is between 1000 – 1300 cm-1 [33, 37, 40, 41]. This region can be further separated into cyclic (~ 1080 cm⁻¹) and linear (~1030 cm⁻¹) regions to denote the structure of the bonds [42]. Though it is very slight, linear Si – O – Si peak is present in the aqueous formulations though it lacks a cyclic peak implying the existence of predominantly linear sol-gel structures formed

within. Furthermore, in the 5 and 10 % v/v TMOS gel, the presence and intensity of cyclic peaks agrees with the observed condensation of denser gels.

2. Nanoparticle Suspension Analysis

Condensation of precursor molecules into solid particles occurs at different rates and with different resulting structures depending on temperature, pressure, pH, and any catalysts used. For the purpose of creating an easily prepared room temperature biomolecule storage technique, only pH and catalyst parameters were explored.

To measure the effects of pH and catalysis on hydrolysis of precursor and subsequent network formation, dynamic light scattering (DLS), pH, and zeta potential measurements were taken on 0.5 % v/v TMOS samples that were hydrolyzed with and without buffer (Tris 33 mM, EDTA 3.3 mM), salt (NaCl 50 mM), and a combination of the two. With 24 hours of settling time after hydrolysis measurements were taken on the dispersion of silica nanoparticles and the resulting data can be seen in TABLE III below.

TABLE III

NANOPARTICLE SUSPENSION SOLUTION PROPERTIES

Sample	DLS (nm)	Polydispersity Index (PDI)	Zeta Potential (mV)	pH
0.5 % v/v TMOS	35.7 ± 1.6	0.383 ± 0.001	-23.45 ± 1.92	6.00
0.5 % v/v TMOS, NaCl	73.1 ± 0.3	0.118 ± 0.007	-4.65 ± 5.41	5.61
0.5 % v/v TMOS, TE buffer	92.2 ± 3.5	0.331 ± 0.032	-30.10 ± 1.91	7.28
0.5 % v/v TMOS, TE buffer, NaCl	120.4 ± 0.3	0.186 ± 0.02	-13.24 ± 1.17	7.15

The data shows a clear trend in nanoparticle formation at these *CaRGOS* formulations indicating the role these additives are playing in each system. Using the 0.5 % v/v TMOS formulation as a baseline for particle formation and zeta potential, the use

of NaCl as catalyst results in roughly double particle size while also reducing the PDI of the suspension. TE buffer aids in particle growth more substantially than NaCl, nearly tripling in size but offering no significant change in the PDI from a formulation without additives. The combination of both TE buffer and NaCl results in nanoparticles that exceed both additives alone, about four times the baseline sample with half the PDI. The results that can be gleaned from particle size analysis are that both additives aid in formation of larger nanoparticles, buffer has a greater effect on particle formation of more varying sizes, while salt has a lesser effect but creates a more uniform distribution. The reasoning behind these results can be attributed to the effects salt and buffer have on the polymerization mechanism for nanoparticle formation. Both salt content and pH levels affect the polymerization of silica sol-gels. Inductive and steric factors affect both the hydrolysis and condensation reactions heavily, therefore the salinity and pH of a sol-gel solution will play large rolls in the resulting particles [33].

The formation of silica nanoparticles follows the Stöber method, where controlling the pH ultimately allows synthesis of nanoparticles of controllable and uniform size. As previously mentioned, acidic conditions can catalyze hydrolysis reactions by increasing Si atom susceptibility to backside attack by water or hydroxyl groups expediting hydrolysis. However, because silanol has an isoelectric pH in the more acidic regime, the condensation reaction is more reversible resulting in smaller, less branched nanoparticles. In the more alkaline regime (pH 7 – 10) the deprotonation of silanol hydroxyl groups creates a far more competitive environment for nanoparticle formation through Ostwald ripening where the larger nanoparticles dominate precursor consumption while smaller nanoparticles that manage to form dissolve and feed larger particles [31]. It is seen in the

collected data that the PDI of sol-gel dispersions of 0.5 % v/v TMOS precursor with pH modification alone are sizable in comparison to the formulations with NaCl added, regardless of pH. The addition of salt increases the rate of the Ostwald ripening of the larger primary particles, allowing for the development of ultimately uniform nanoparticles in shorter times, explaining the smaller PDI in both cases where NaCl is present.

Zeta potential of a colloidal suspension is indicative of a collection of suspended particles to aggregate and collect within a solution and is imperative to the stability of a biomolecule adsorbed to a nanoparticle's framework. There are well accepted regimes of zeta potential that indicate the stability and tendency towards aggregation in solution [43-46]; poor stability (0 – 10 mV), fair stability (10 – 20 mV), good stability (20 – 30 mV) and excellent stability (> 30 mV). To reduce the interaction with negatively charged biomolecules, a more negative zeta potential is preferable. The results show that salt drastically reduces stability while TE buffer adds stability. The use of both additives together brings the solution stability to a fair level, overall reduced from both the basic formulation and the buffered formulation, but acceptable for trials to store biomolecule samples.

3. Two-Step Rapid Nanoparticle Growth

With the effects of salt and buffer explored during hydrolysis and ultimate nanoparticle formation, a more rapid and efficient recipe could be created. The pH conditions induce limiting factors to the system. The use of the Stöber method to hydrolyze TMOS at acidic pH and then introduce buffer and salt afterwards to catalyze condensation was explored. To see the effects of buffer and salt addition after hydrolysis, a 1.25 % v/v TMOS solution was hydrolyzed without salt or buffer and DLS

measurements were taken immediately after hydrolysis and after addition of salt and buffer, bringing the final silica precursor concentration to 0.5 % v/v TABLE IV.

TABLE IV

SOLUTION PROPERTIES OF SOL-GEL BEFORE AND AFTER ADDITIVES.

Sample	DLS (nm)	PDI	Zeta Potential (mV)
TMOS w/out TE Buffer (1.25 % v/v)	*0.79 ± 0.11	0.983 ± 0.026	-22.07 ± 1.01
TMOS with TE Buffer and Salt (0.5 % v/v)	67.22 ± 1.65	0.248 ± 0.006	-10.50 ± 1.66
* Hydrodynamic size <1 nm is insignificant			

The addition of catalyst and buffer after hydrolysis of TMOS shows significant particle growth immediately. Compared to the results from hydrolysis with and without catalyst and buffer, the two-step formulation shows much more efficient particle formation in a shorter period. As stated previously, it has been speculated that at protonated silane and TMOS molecules have less affinity for network formation and aggregation than deprotonated counterparts while the reverse is true for hydrolysis [31]. The observed increase after addition of buffer and resulting rise in pH from 4.66 to 7.07 supports this claim. The pH swing is convenient because silica precursor naturally has a pH of 4.66 after initiating hydrolysis, making it a more ideal environment for fast and complete hydrolysis of TMOS precursor. After hydrolysis, no significant particle formation was observed through DLS measurements and a stable zeta potential was observed suggesting unfavorable conditions for nanoparticle formation. Once buffer and salt are added the pH becomes more neutral at 7.07 and a hydrodynamic size of 67.22 nm is detected with a good PDI and fair zeta potential. This spike suggests an immediate

formation of substantial nanoparticles that have quickly reached later stages of Ostwald ripening as depicted in Figure 5.
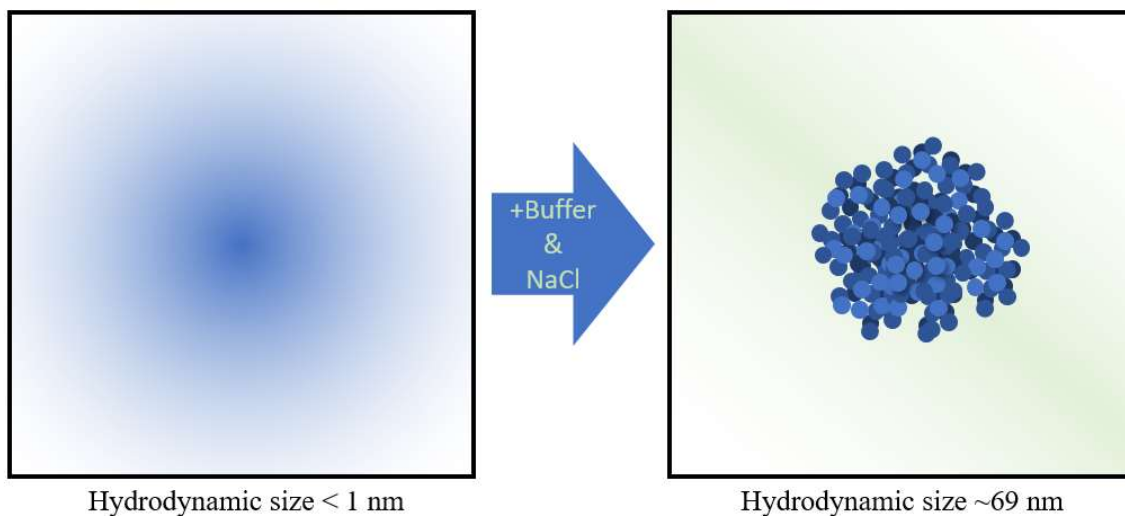
FIGURE 5 – Ostwald Ripening of Silane Precursor

D. Long-Term Stability

This new method of hydrolyzing TMOS was explored using Raman spectral analysis at different steps of the process. Figure 6 shows the Raman spectra observed for 1.25 % v/v TMOS after dispersion and before microwaving (orange trace), after 15 and 30 seconds of microwaving (green or red trace respectively), after degassing methanol for 5 minutes (dark blue trace), *CaRGOS* solution immediately after adding buffer (upper light blue trace), and *CaRGOS* solution after two weeks under ambient conditions (lower light blue trace).
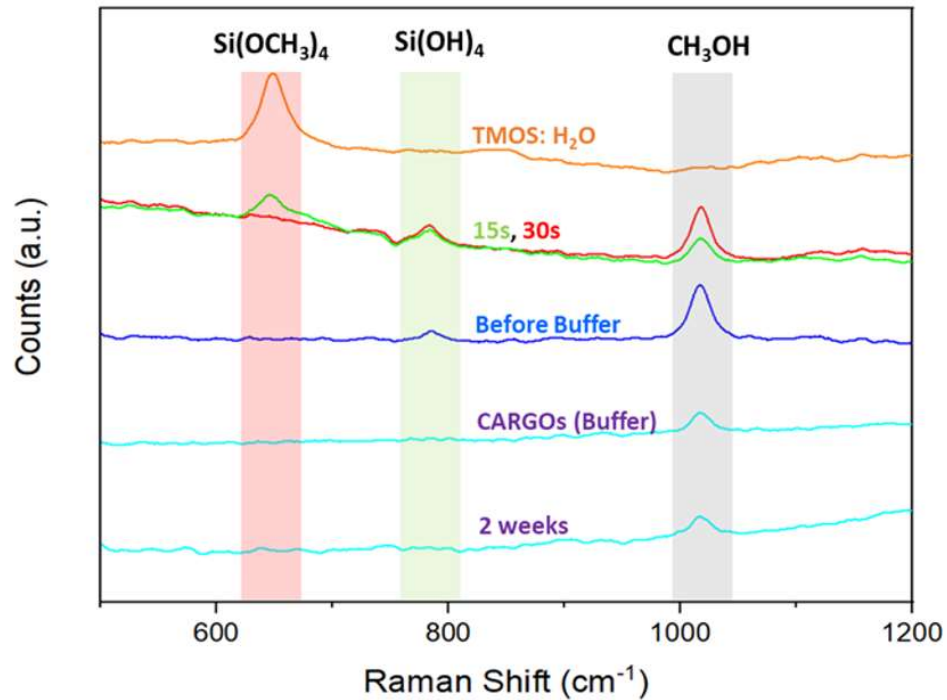
FIGURE 6 – Raman Analysis of CaRGOS Composition Over Time

The presences of various components are signified by peaks at the following Raman shifts:

- TMOS precursor: 640-650 cm^{-1}[31]

- Silicic acid and/or sol-gel dimer: 750-780 cm^{-1}[31]

- Methanol: ~1033 cm^{-1}[31]

Going from the top curve representing the unhydrolyzed mixture to 15 and 30 seconds of microwaving, the TMOS peak rapidly disappears signifying full hydration. Additionally, as the TMOS peak shrinks, the representative peak for silicic acid and sol-gel dimers grows after microwaving. Upon addition of TE buffer, the sol-gel concentration becomes very dilute and disappears almost entirely from the spectrum. The growth and consistency of the methanol peak indicates the presence of the species in *CaRGOS* solution even after off-gassing and dilution.

V. Conclusions

By employing microwaves to induce TMOS hydrolysis, it has been shown that it is possible to synthesize biocompatible silica gels and nanoparticles. Within 30 seconds of exposure to microwaves from a common microwave unit, up to 10 % v/v TMOS formulations have been hydrolyzed with near 100% efficiency. FTIR measurements on the hydrolyzed solutions shows successful formation of ordered structures within sol-gels prepared in this method at concentrations between 0.5 – 10 % v/v TMOS. Using Raman analysis of Methanol concentration immediately after hydrolysis of TMOS precursor, it has been shown that even in the case of 0 % methanol evaporation, a majority of alkoxy ligand separation has been achieved.

While hydrolysis was shown to be nearly complete at up to 10% v/v TMOS precursor concentration with microwaves alone, the condensation of resulting silanol molecules has been further improved with solution parameters. With modification of pH and saline concentration, the Ostwald ripening process of primary nanoparticles has been seen to progress after only 24 hours. Nanoparticle sizes of up to ~ 120 nm were achieved when hydrolysis and condensation were performed in 50 mM NaCl and 33 mM TE buffer (pH 7.4).

Further experimentation was done to explore the hydrolysis and condensation mechanism if he two were carried out under two separate steps. Under naturally acidic conditions, the hydrolysis of 1.25 % v/v TMOS occurred rapidly and upon dilution with TE buffer and NaCl ~ 69 nm nanoparticles were observed immediately. With fair zeta potential of -10.5, this solution would be ready to add a biomolecule after less than 15 minutes of total synthesis time. Additionally, raman measurements of 0.5 % v/v sol-gel

CaRGOS over 2 weeks shows solution stability over extended periods of time, suggesting that this formulation could be used for long term storage. In conjunction with the optical clarity observed in *CaRGOS* at various sol-gel concentrations over extended time, it is entirely possible to move forward to testing with real biomolecules over extended time while non-invasively assessing their integrity.

RNA CARGOS

OVERVIEW

This section will recount the investigation of room-temperature integrity preservation of miRNA 21, which is a potential biomarker of tissue toxicity, cancer diagnosis, regulator of cancer immunotherapy biomarkers [6, 8] and down-regulator of multi-drug resistance (MDR) transporters[47, 48]. The sterile *CaRGOS* are achieved utilizing a deliberately low concentration of TMOS/water suspension that is hydrolyzed in a standard microwave. Biospecimen of interest can be added to the hydrolyzed silica at room temperature, resulting in its stabilization. In this study, the room temperature integrity, preservation, cancer immunotherapy and multi-drug resistance (MDR) regulation challenges using a representative highly sensitive bioanalyte miRNA 21 have been addressed. Specifically, a single-step ~ 100 % recovery of miRNA 21 at room temperature using aqueous formulations of *CaRGOS* with extremely low silica concentrations (0.5%) has been demonstrated. The aqueous formulations of the *CaRGOS* with biospecimen are significantly versatile for downstream processing than conventional sol-gel matrices with immobilized biomolecular entities that require physical forces to overcome the non-covalent interactions, with a strong likelihood of rupturing biological activity before downstream usage[49-51]. Moreover, the technique is completely compatible with a host of proteins as well as other nucleotides such as DNA.

Although stabilization of biomolecular entities emanates from their restricted rotation or immobilization within the silica matrices, yet the highly aqueous formulations lacks the concentration-range requisite for such immobilization. Therefore, to validate the mode of stabilization of biospecimen in highly aqueous formulations of *CaRGOS* matrices, the inherently dual nature of silica precursors: immobilization and nuclease-

27

inhibition, have been investigated. In highly-stable *CaRGOS* formulations, a remarkable resistance to nuclease (i.e., RNase A) was observed by demonstrating ~0 % quenching of Ethidium bromide, thereby protecting ~100% integrity of yeast RNA. Also in this section, it is shown that a ~ 69 nm hydrodynamic- sized aqueous formulation of *CaRGOS* efficiently preserves miRNA 21 up to 28 days at above-freezing temperatures (4, 25, 40) °C with ~100% single-step recovery. The aliquots from *CaRGOS* sol-gel/miRNA 21 solutions have demonstrated fluorescence quenching of chemotherapeutic drug doxorubicin supporting a realizable immunoadjuvant potential of silica matrices and MDR circumvention by miRNA mimics[6, 8, 52, 53].

II. Instrumentation and Equipment

A. Infrastructure and Equipment

Sterile laminar hood

Fume hood

Microwave 1200 Watt with viewing window in order to monitor samples during use.

Vortex machine

Dynamic Light Scattering (DLS) machine

Thermocycler for reverse transcriptase of miRNA (TaqMan MicroRNA Reverse

Transcription Kit)

Quantitative polymerase chain reaction (qPCR) machine

Reva Educational Raman platform.

Micropipettes capable of measuring as little as 0.5 uL

Sealable glass vessel with 2-3 ventilation holes in the cap for gasified methanol

B. Chemicals

Tetramethyl orthosilicate 99% (TMOS) from Acros Organics.

Ethidium bromide from Sigma Alderich.

Nuclease free water (NFW)

Tris-EDTA (TE) buffer from Sigma Aldrich.

Sodium Chloride (NaCl) from Sigma Aldrich.

miRNA 21 from IDT.

Yeast RNA from IDT.

III. PROCEDURE

A. Sample Preparation

1. Buffer

Sol-gels alone do not inherently provide an accommodating environment for biomolecules. In order to finely tune the mixtures to be more habitable for the samples, buffers are added to control pH and add stability within silica networks.

For ideal miRNA storage, a buffer is necessary to create a habitable environment. The buffer consisted of saline solution with varied concentrations of NaCl between 75 and 250 mM, 5.0 mM Tris-HCl (pH 7.5) and 0.5 mM EDTA which was prepared by bringing the salt concentration of a store-bought Tris-EDTA (TE) buffer to the appropriate level and then diluting by half.

CaRGOS solution is prepared by combining a pure hydrolyzed TMOS solution of

the desired % v/v, a buffer solution, and the sample to be stored. Once both sol-gel and

buffer are prepared, they are combined in a 1:2 ratio for a final concentration of one third

initial sol-gel, 50 to 166 mM NaCl, 3.3 mM Tris-HCl, and 0.33 mM EDTA. RNA

specimen is thawed from cryogenic storage and added to *CaRGOS* for an analyte

concentration of 500 nM. Figure 7 below depicts a schematic of the *CaRGOS* synthesis

procedure.
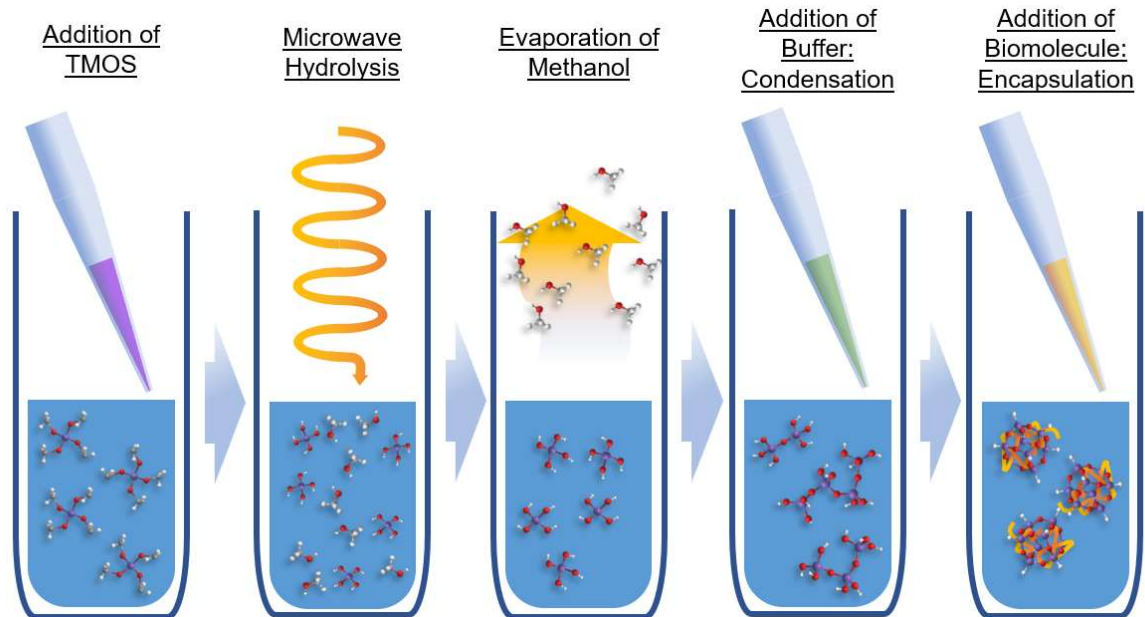
FIGURE 7 – Biomolecule *CaRGOS* Preparation Process

3. Reverse Transcription Recipe

A master mix was prepared before reverse transcription (RT) of the analyte was performed using TaqMan MicroRNA Reverse Transcription Kit components. The master mix recipe is presented in Table V.

TABLE V

MASTER MIXTURE RECIPE PER WELL FOR RT OF MIRNA 21

Component	Volume (μL) per well
100 mM dNTPs	0.15
MultiScribe Reverse Transcriptase, 50 U/μL	1.00
10X Reverse Transcription Buffer	1.50
RNase Inhibitor 20 U/μL	0.19
Nuclease-free water	4.16
5X miRNA Primer	3.00
Total volume (μL)	**10.00**

RT components and 5X miRNA Primer were thawed from freezing and vortexed before combining. Once the master mix was prepared, 10 µL was pipetted into one well in a 200µL 96-well reaction plate for each desired reaction. 5 µL of each miRNA sample to be analyzed was pipetted into a well with master mix which was subsequently capped and mixed gently in order to settle the solution towards the bottom of the wells. The 96-well reaction plate was then incubated on ice for 5 minutes before being transferred to an Eppendorf thermocycler at 85 °C for 65 minutes.

4. Real-time qPCR Amplification Recipe

Much like RT, a master mix was prepared and distributed on a reaction plate before the samples were ready to be added and analyzed. The master mix recipe for qPCR for the volume in each well is listed in Table VI below.

TABLE VI

MASTER MIXTURE RECIPE PER WELL FOR RT-QPCR

Component	Volume (μL) per 10-μL reaction
20X miRNA Primer	0.5
Universal Master Mix	5.00
Nuclease-free water	3.17
Total Volume	**8.67**

8.67 µL of master mix was prepared in individual wells of a 100 µL PCR 96-well reaction plate for each sample analyzed. 1.33 µL of RT product was pipetted into its respective well on the PCR 96-well reaction plate which was subsequently sealed and gently mixed to ensure the solution was resting at the bottom of the well before running real-time qPCR.

B. Experimental Procedure

1. CaRGOS Solution Stability With RNA.

DLS and zeta potential measurements were taken on 1.25 % v/v sol-gel solution before and after being mixed to create the final *CaRGOS* solution. A 1.25 % v/v sol-gel was prepared in the manner described in the sample preparation section and allowed to settle for some time before initial measurements were taken. TE buffer and miRNA 21

were then added and a second set of measurements was taken. This was done in order to measure the size, dispersity, and stability of the silica sol-gel and track changes to the network with the addition of buffer and RNA specimen.

2. TMOS Concentration Analysis.

This new sol-gel method for miRNA storage requires neither catalysts nor cosolvents, which is favorable for further study on how the silica network and the specimen interact. The effect of concentration and density of the silica in solution was analyzed by introducing miRNA into 5 sol-gel solutions prepared with varying v/v % TMOS precursor. A 20 % v/v TMOS mixture was hydrolyzed, and then through serial dilution, solutions of 10 %, 5 %, 2.5 %, and 1.25 % were created and then combined with TE buffer and NFW before spiking the solutions to ~500 nM miRNA 21. The recovery of intact miRNA from the samples was quantified via RT, qPCR, and a calibration curve available in APPENDIX I Figure 18.

3. Salinity Analysis.

Salt concentration is a key factor in both the sol-gel process and in the stabilization of genetic materials. A more saline solution is preferable for sol-gel synthesis but detrimental to the survival of RNA. Using a 1.25 % v/v TMOS sol-gel and the *CaRGOS* formula described above, while varying the NaCl concentration between 0.15 M and 0.5 M, two sets of *CaRGOS* samples were prepared. The two sets of *CaRGOS* solution were spiked to ~500 nM miRNA 21, and their stability was measured using RT and qPCR.

4. Time and Temperature Study.

Three sets of *CaRGOS* solution were prepared with 1.25 % v/v silica precursor and 0.15 M NaCl buffer. These samples, as well as a control sample without *CaRGOS*, were

spiked to ~500 nM miRNA 21. One of the *CaRGOS* and the control sample were kept at room temperature (25 °C), one *CaRGOS* was kept at elevated temperature (40 °C), and the last *CaRGOS* was refrigerated (4 °C) for four weeks. An aliquot of each sample was taken for quantification by qPCR at times of 1 day, 1 week, 2 weeks, 3 weeks, and 4 weeks after addition of miRNA.

5. Nuclease Inhibition Analysis.

Florescence emission measurements were used to study the shielding properties of *CaRGOS* in the presence of aggressive proteases and nucleases. *CaRGOS* solution was spiked with yeast RNA, bound to Ethidium bromide, to 1 mg/ml (0.077 M), and bovine pancreatic RNase A was added at incremental concentrations from 0 to 1200 nM. This experiment illustrated the *CaRGOS* technology's capacity to defend against aggressors of biological materials. The fluorescence of the mixture and a control buffer without *CaRGOS* was monitored using a Zetasizer Nano ZS90.

IV. RESULTS AND DISCUSSION OF RESULTS

A. *CaRGOS* Solution Stability With RNA

Ideally the network formation of sol-gel should occur within a short period of time before the addition of the specimen. The silica nanoparticle formation was tracked with DLS hydrodynamic size measurements with and without the addition of the TE buffer and miRNA 21. Before the addition of the buffer and sample, a hydrodynamic radius of ~1 nm was observed in the sol-gel mixture, which changed to ~70 nm after their addition. Full display of DLS, polydispersity index, and zeta potential measurements are displayed in Table VII.

TABLE VII

DLS, PDI, & ZETA POTENTIAL MEASUREMENTS

Sample	DLS (nm)	PDI	Zeta Potential (mV)
CaRGOS w/out TE Buffer (1.25 % v/v)	*0.79 ± 0.11	0.983 ± 0.026	-22.07 ± 1.01
CaRGOS with TE Buffer and miRNA (0.5 % v/v)	69.95 ± 0.47	0.308 ± 0.004	-20.04 ± 1.26
* Hydrodynamic size <1 nm is insignificant			

This observation falls in line with the reported trend [31] that silica sol-gel nanoparticles aggregate more effectively at near neutral pH. Once introduced to the buffer, the silica precursors have a stronger drive to form around and restrict the miRNA backbone.

B. Salinity and pH

Fluctuations in salt concentration as well as pH are well documented as being detrimental to RNA but necessary for the formation of sol-gel nanoparticles over time. To curb the effects of pH on miRNA 21, an as-bought TE buffer was utilized to maintain a constant pH environment even in the presence of acidic silica precursor. Salt concentration aids in the sol-gel aggregation process but could prove harmful to a sample in too-high a concentration. Also, salinity has a ubiquitous effect on non-covalent interactions between biospecimens and *CaRGOS* matrices. Previously, Buijs et.al. had reported an electrostatic adsorption induced destabilization of proteins (e.g. RNase A/Lysozyme) on 11 nm silica particles[54]. They had observed a superior electrostatic attraction between proteins and silica nanosystems in low ionic strength buffer solutions, compared to their high ionic strength counterpart environments. The high ionic strength environment could significantly reduce the electrostatic attraction between the negatively charged silica nanosystem and any positively charged RNase from environmental contamination. Therefore, miRNA 21 storage and downstream processing in high salt environment is highly susceptible to miRNA degradation via RNase contamination. After preparing, processing, and analyzing *CaRGOS* solutions with 1.25 % v/v precursor and NaCl concentrations of 0.5 M or 0.15 M, it was found that the lower saline TE buffer returned comparable critical threshold (C_T) values as the original 1.25 % v/v while introducing more consistent stability to the system. The mean C_T values can be seen in Figure 8.
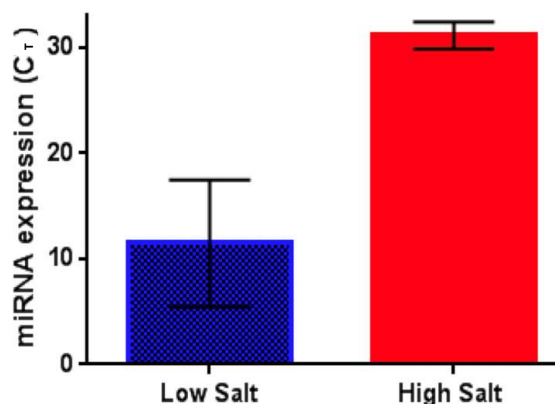
FIGURE 8 – Mean C_T Values of Low (0.15 M) and High (0.5 M) NaCl *CaRGOS*

In response to salt stress, the miRNA expression levels were $C_T = 31.1 \pm 1.2$ and were $C_T = 11.5 \pm 6.0$ in high salt and low salt buffers respectively, which demonstrates miRNA 21 instability in high saline environments. Therefore, the undetermined miRNA 21 levels in the high salt buffer environment were attributed to the (a) miRNA21 instability induced by RNase, present in the environmental contamination and (b) absence of electrostatic adsorption induced destabilization of positively charged RNase on negatively charged *CaRGOS* surface.

C. Effects of Silica Concentration

In order to determine the ideal recipe for *CaRGOS*, sol-gels were prepared with different concentrations of TMOS precursor, and equal amounts of miRNA were added to each set. Solutions with concentrations of 20 %, 10 %, 5 %, 2.5 %, and 1.25 % TMOS were prepared, and each was spiked to miRNA 21 concentrations of ~500 nM. After addition of analyte, aliquots were taken from each sample set and processed via RT using a thermocycler and an RT precursor kit. Once completed, the samples were then analyzed using qPCR amplification with an applied 0.1 C_T threshold. All readings $C_T > 30$ were

considered to be NFW or minute contaminant contributions. Concentrations of miRNA 21 in *CaRGOS* were determined through mean C_T values compared to standard calibration curve Figure 19 in APENDIX I. Figure 9 shows the measured pH and miRNA 21 concentration of each *CaRGOS* formulation made with varying TMOS precursor concentrations.
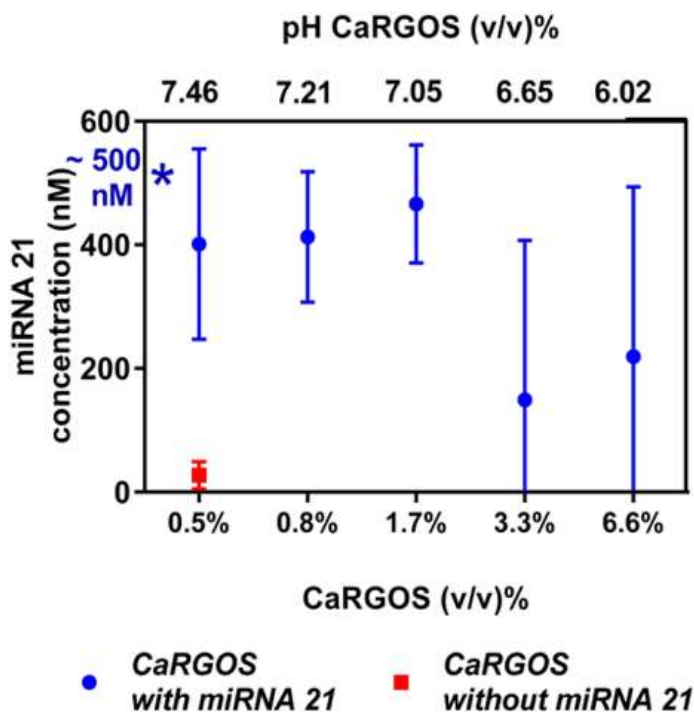
FIGURE 9 – Precursor Effects On pH & miRNA Recovery

The results of the TMOS precursor study were mixed. At higher concentrations it was apparent that miRNA 21 preservation and recovery is neither easy nor viable. The final *CaRGOS* product at higher concentrations is either a solid gel or a viscous fluid from which sample recovery is difficult. The mechanism of stabilization of the miRNA is a balanced combination of non-covalent interaction of the miRNA backbone with parts of the silica sol-gel matrix, and favorable solution conditions with minimal interaction with

the sample [28, 49, 55-57]. As the concentration of silica sol-gel increases, the balance is shifted, and miRNA becomes less stable and recoverable from the solution. Increasing the concentration of the sol-gel provides excessive restriction and immobilization of the miRNA, to a point where separation and recovery is difficult and potentially harmful to the sample[49]. At concentrations of 1.7 % v/v, 3.3 % v/v, and 6.6 % v/v the resulting *CaRGOS* was too viscous and gel-like for single step recovery so separation by centrifuge had to be employed. The stress of separating the miRNA backbone from a dense silica network could easily break the molecule apart [58]. Additionally, the higher concentration of sol-gel drops the pH of the *CaRGOS* to less habitable levels making denaturization of the miRNA sample entirely possible while within the sol-gel matrix.

The lower two concentrations of silica sol-gel required no additional steps to recover a quantifiable sample, all that was needed was a sterile pipette. This single step recovery of high miRNA concentrations is preferable for a final, easy to use product. The small amount of equipment and infrastructure required for sample storage, transport, and recovery with *CaRGOS* is one of the qualities that sets it apart from most other methods used [1, 2]. Between the two lower concentration formulations, 0.5 % v/v maintained its low viscosity over long periods of time, where the 0.8 % v/v *CaRGOS* gradually became more gel-like as time progressed due to the continued formation of silica sol-gel network within the solution.

It was determined that experiments would proceed with the 0.5 % v/v TMOS formulation because, though not quite as effective as some of the higher concentrations, this formulation facilitated sample recovery due to its lower viscosity.

D. Time and Temperature Study

To assess the validity of this new method, sample sets of ~500 nM miRNA with

CaRGOS were prepared and held at 4, 25, and 40 degrees Celsius, while another set of

500 nM miRNA 21 without *CaRGOS* was left at 25 degrees for comparison. At times of

1, 7, 14, 21, and 28 days, aliquots from each sample set were characterized using qPCR.

Figure 10 below shows the results of the miRNA recovery from all samples at each time

step.
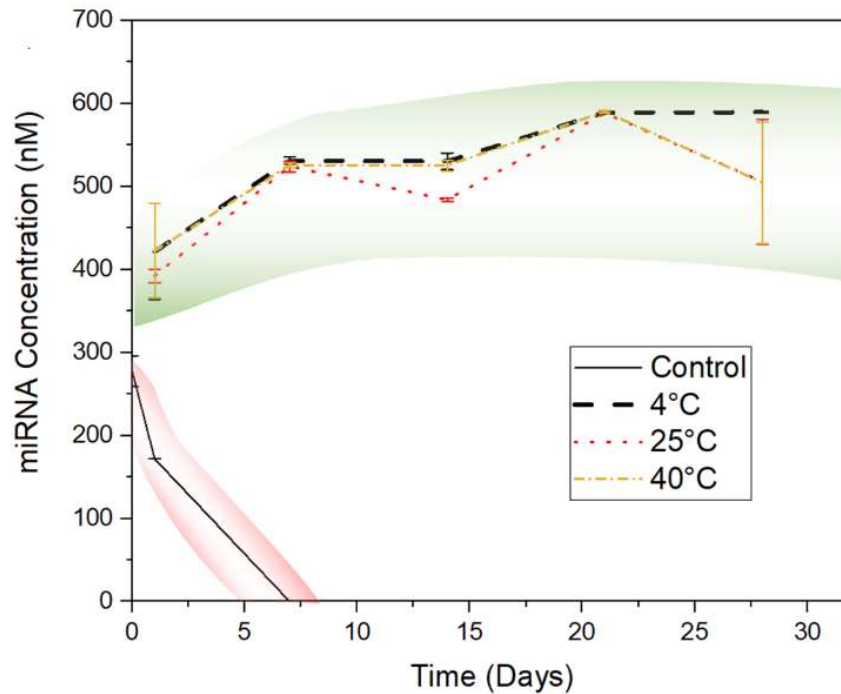
FIGURE 10 – miRNA Recovery from *CaRGOS* at 4°, 25°, & 40°C

The control sample at room temperature was measured on initial day of storage after

brief incubation at room temperature. After less than one day at room temperature, the

control sample without *CaRGOS* loses roughly half initial miRNA concentration

illustrating the instability of miRNA. One full day of room temperature incubation

sharply decreases the concentration within the control sample, and by the first week the miRNA was entirely depleted. *CaRGOS*, on the other hand shows very favorable preservation of the miRNA over the full 28 days at all temperatures.

Initial measurements of *CaRGOS* samples at the three temperatures appeared slightly concerning, showing preservation of less than 100% of the starting miRNA 21 concentration after one full day of incubation with a high standard deviation. After 7 days, the values of miRNA appeared to increase from the first measurements. Subsequent sets of measurements provided fluctuating mean C_T values, increasing and decreasing noticeably between weeks. Though odd, the trend of increasing and decreasing on particular days is shared between all temperature sets. It is assumed that the fluctuation, standard deviation, and overall increase in C_T values is due to the gradual release of methanol in the solutions over time [59]. This explains the standard deviation of the 1-day measurements across all temperatures that is otherwise not present during subsequent measurements. The methanol concentration would be highest during the first day and would be significantly lower after 7, 14, 21, and 28 days. Additional increase in standard deviation is observed at 28 days for 25° and 40°C. Regardless of fluctuations, measured C_T values and resulting calculated concentrations of miRNA 21 in *CaRGOS* solutions at all temperatures provided preservation of ~100% initial sample concentration with easy single step recovery at each time.

Comparison shows, irrefutably, that *CaRGOS* guarantees preservation of miRNA 21 at a wide range of temperatures with little to no signs of degradation, while the sample without *CaRGOS* showed immediate degradation after one day and total denaturization after one week.

E. Shielding Capacity

Resulting fluorescence measurements from the incremental increase of RNase A into *CaRGOS* are indicative of the shielding properties of the solution. Figure 11 plots out the relative fluorescence of *CaRGOS* and control buffer solutions when introduced to a range of RNase A concentrations between 0 and 320 nM.
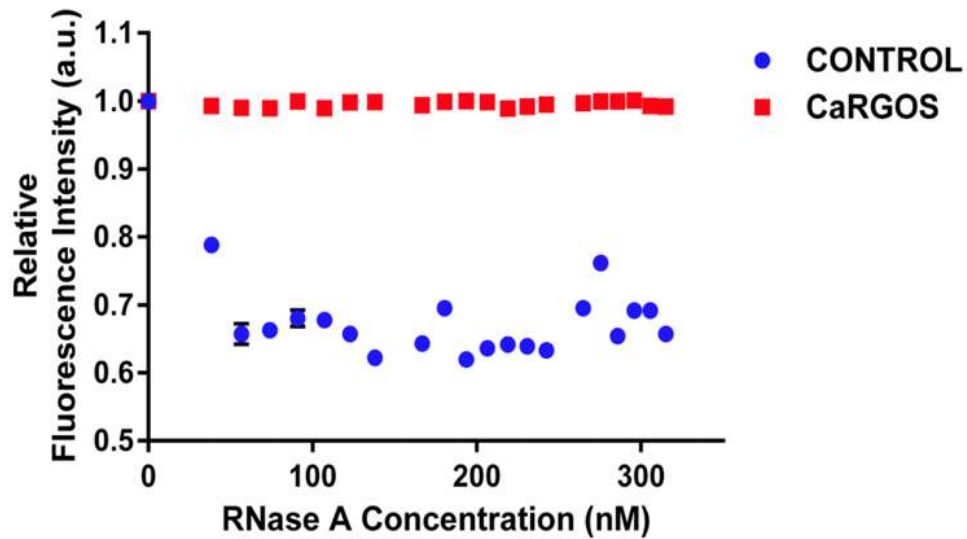
FIGURE 11 – Fluorescence Measurements for 0 to 320 nM RNase A

When EtBr is intercalated with nucleic acids it increases in fluorescence dramatically making it an ideal dye to enhance the fluorescence of RNA for analysis. When the molecule EtBr is bound to is denatured in any way, the fluorescence decreases markedly, which would facilitate the monitoring of RNA integrity under different conditions. In this study, the relative fluorescence of EtBr bound to yeast RNA was monitored in samples with and without 0.5% v/v *CaRGOS* that were exposed to increasing amounts of RNase A, a compound with the specific purpose of attacking and denaturing RNA from foreign sources such as viral exposure. The integrity of the RNA is correlated with the

fluorescence observed with the addition of RNase A relative to the original fluorescence of pristine RNA.

A trend is clearly illustrated in Figure 11 as the control samples undergo a relative fluorescence quenching of roughly 40% while *CaRGOS* is, for the most part, unperturbed as the RNase A concentration increases. Comparing relative fluorescence measurements at each RNase concentration indicates that *CaRGOS* is providing total protection of the RNA where it would otherwise suffer from attack by RNase.

The observed trend is attributed to RNase A inhibition by the *CaRGOS* solution via electrostatic adsorption [24, 25, 60-62]. The general mechanism of RNA denaturization via RNase attack is cleaving of the backbone at the Phosphorus in the backbone. RNase is drawn to the RNA by electrostatic attraction between positively charged acid groups or metal ligands on RNase to the negatively charged region of the RNA [54]. When bound to silica sol-gel, however, RNase is deflected from attacking RNA and instead binds to the net negative regions of silica and is destabilized. Figure 12 depicts an RNase molecule attempting to attack strand of RNA nested inside a sol-gel network only to be disarmed.
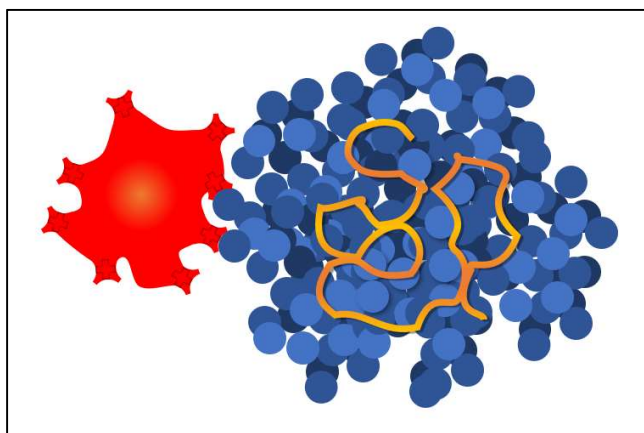
FIGURE 12 – *CaRGOS* RNase Inhibition and RNA Protection

44

Though both RNA and the silica sol-gel are net negatively charged, the silica associates with the backbone and non-covalently binds with it colinearly [27]. The presence of silica on and around the RNA provides excellent steric support as well as a nearly impenetrable chemical defense to the otherwise unstable and vulnerable biomolecule.

At RNase A concentrations higher than 320 nM however, the fluorescence increased as shown Figure 20 in APPENDIX I. This increase in fluorescence is due to the sheer amount of RNase A present, and EtBr binding with the silica network as well as the remaining RNA [63, 64].

F. Immunotherapeutic Potential

Both components of the highly optimized aqueous formulations, *CaRGOS* (0.5 % v/v) and miRNA 21, have potential as immunostimulants [19, 27, 48]. Previously, Cha et.al. displayed the immunotherapeutic potential of mesoporous silica nanoparticles (20-30 nm) against melanoma using a model tumor antigen [26]. Wang and Chen et.al had also reported a significant immunoadjuvant effect with these irregularly porous silica nanoparticles by encapsulating antigens and danger signal immunological molecules (DAMP: damage associated molecular pattern) in their extra-large pores [6, 19]. Similar to these tunable mesoporous silica nanoparticles, large-sized *CaRGOS* nanosystem (~ 69 nm) with its excellent buffer dispersions stability could be suitable as an immunostimulant agent.

Furthermore, miRNA 21 molecules have been known to act as biomarkers in cancer immunotherapy, regulating expressions of programmed death ligand (PD-L1) in colorectal cancer [6, 8]. Consequently, miRNA 21 solutions in highly optimized aqueous

formulations of the *CaRGOS* nanosystem could be potential immunostimulants in cancer immunotherapy. With its thermal and chemical stability over long periods of time availability and performance of drug availability and delivery.

The anthracycline doxorubicin (DOX) has strong synergistic interactions with DNA/RNA and has a downregulating effect on immune checkpoint inhibitors (e.g. PD-L1) [65, 66]. Zhu et. al. had demonstrated a multi-drug circumvention (MDR) strategy by controlling the intracellular release of DOX using miRNA 16 mimics [53]. Also, Rubio et.al. observed doxorubicin (DOX: Emission: 560-590 nm) fluorescence quenching after DOX intercalation into RNA mimics [53, 65].
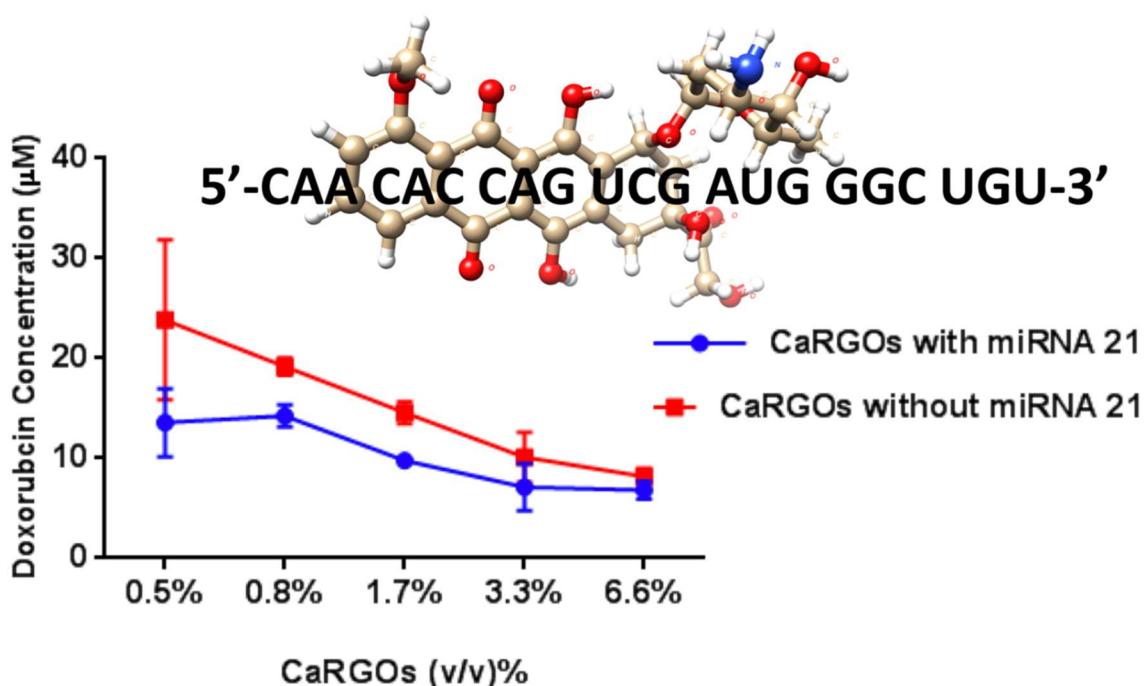
FIGURE 13 – Doxorubicin Quenching in *CaRGOS* with and without miRNA 21

As shown in the Figure 13, the DOX (50 µM) fluorescence quenching was observed with *CaRGOS* [(0.5 – 7.0) % v/v; (pH: 6.0 - 7.5)] samples with and without miRNA 21. This displays the combined effect of (a) DOX's non-covalent interaction

with miRNA 21 and (b) DOX's intercalation into the *CaRGOS* silica matrices [53, 65]. DOX concentrations were similar at higher *CaRGOS* concentrations [(3.0 - 7.0) % v/v; pH < 7] with and without miRNA 21, while a differential response of DOX fluorescence quenching (9.6 – 17.0) μM was observed at lower *CaRGOS* concentrations [(0.5 – 1.7) % v/v; pH > 7]. Such fluorescence quenching at lower *CaRGOS* concentration gradient is attributed to the non-covalent DOX-miRNA interaction and a synchronized DOX – *CaRGOS* intercalation, indicating the perseverance of the miRNA 21 integrity in such *CaRGOS* aqueous formulations. On the other hand, the similar DOX concentration levels in higher *CaRGOS* concentrations [(3.0 - 7.0) % v/v; pH < 7] indicates loss of miRNA 21 stability in their aqueous media. The DOX concentrations (μM) of *CaRGOS* samples were evaluated by measuring mean fluorescence values (FL) using standard calibration curves at modulus fluorimeter (Green module: Emission: 580 - 640 nm), APPENDIX I Figure 21. Therefore, the aliquots of *CaRGOS* (0.5 wt./v %) based aqueous formulations with their DOX/miRNA 21 suspension could potentially demonstrate adjuvant effect in cancer immunotherapy or macromolecular (*CaRGOS*/miRNA) conjugation induced multidrug resistance effect respectively [19, 26, 53, 63, 67].

V. CONCLUSIONS

CaRGOS has proven to be a novel, quick, and easy formulation which facilitates long-term storage and preservation of miRNA 21 at refrigeration, room, and elevated temperatures while allowing quick, easy, and complete recovery. The environment created within *CaRGOS* allows for non-covalent interaction within the silica nanoparticles that restricts the movement of the miRNA backbone, while at the same time inhibiting harmful RNase and contaminant interaction with the sample. Fine-tuned pH, low ionic strength, and their large hydrodynamic size are attributes that lend themselves to the denaturing of contaminants harmful to miRNA. Recovery of miRNA over several weeks at room and elevated temperatures shows that the natural inclination for unstable biomolecules to denature themselves is being suppressed within the silica network. This method shows unique and well-rounded protective measures. Being long lasting under a variety of otherwise unfavorable temperatures, while so easy to prepare, makes *CaRGOS* an invaluable tool for research of biomolecules.

HEMOGLOBIN *CARGOS*

OVERVIEW

Metalloproteins, in general, are greatly associated with human health. Hemoglobin binds and transport analytes (i.e., oxygen, nitric oxide, carbon monoxide) and plays significant role in the regulation of blood pressure. Hemoglobin is a model protein chosen for investigating the preservation of structural integrity under environmental stimuli (heat, mechanical excursions, nuclease/protease/microbial contamination), due to its complex four protein-chain framework, with each chain having heme group and metal center (i.e., iron) in the central cavity. Purified proteins in their native state are known to be slightly disordered and for having certain sections in their unfolded state [68]. Therefore, instead of investigating secondary structures (i.e., α-helix), thermal stability (~ 25 °C) and mechanical handling (mixing, vortexing, shaking) investigations with *CaRGOS*-hemoglobin formulations are focused on the analysis of heme groups of the four-polypeptide chain network of hemoglobin. Previously, Chen et.al. had developed a silica-gel (powder) based room-temperature storage of proteins (i.e., Lysozyme) [27]. However, post-ensilication, the protein - reconstitution in aqueous buffers at room-temperature is partly analogous to a conventional reconstitution of freeze-thawed or lyophilized proteins and therefore could denature the protein nativity. In this paper, the room-temperature stability and mechanical handling of hemoglobin in aqueous *CaRGOS* formulations will be addressed, developing an ambient-temperature based alternative strategy to preserve metalloprotein's nativity, homogeneity, activity and reproducibility over long-term storage.

II. INSTRUMENTATION AND EQUIPMENT

A. Infrastructure and Equipment

Sterile laminar hood

Fume hood

Microwave 1200 Watt with viewing window in order to monitor samples during use.

Vortex machine

DLS machine

UV-Vis spectrophotometer

Centrifuge

Micropipettes capable of measuring as little as 0.5 uL

Sealable glass vessel with 2-3 ventilation holes in the cap for gasified methanol

B. Chemicals

Tetramethyl orthosilicate 99% (TMOS) from Acros Organics.

Nuclease free water (NFW)

Sodium Phosphate dibasic from Sigma Aldrich.

Sodium Phosphate monobasic from Sigma Aldrich.

Potassium Hydroxide from Sigma Aldrich

Polyethylene Glycol from Sigma Aldrich.

Sulfuric Acid from VWR

Polymethylmethacrylate UV-grade cuvettes from VWR.

Freeze dried Hemoglobin from VWR.

III. PROCEDURE

A. Sample Preparation

1. Hemoglobin Stock Solution

A 1%wt stock solution of hemoglobin is used to create all following samples for analysis. Freeze-dried hemoglobin is weighed out into sterile, sealable containers and previously prepared 0.5M NaPb is used to rehydrate hemoglobin. In order to preserve hemoglobin until the time of testing all samples are kept in the refrigerator prior to all experimentation.

2. Phosphate Buffer

In order to provide additional stability to hemoglobin, a 0.5M sodium phosphate buffer (NaPb) of pH 8.20 was chosen. Using a modified Henderson-Hasselbalch Equation, Equation XX, the appropriate amounts of sodium phosphate monobasic, and conjugate base sodium phosphate dibasic were derived.

(Equation XX) $$pH = pK_a + log\frac{[NaP_b]}{[NaP_a]}$$

$$\frac{[NaP_b]}{[NaP_a]} = 10^{(pH - p\ a)}$$

$$[NaP_b] = [NaP_{total}] - [NaP_a]$$

$$\frac{[NaP_{total}] - [NaP_a]}{[NaP_a]} = \frac{[NaP_{total}]}{[NaP_a]} - 1 = 10^{(pH - pK_a)}$$

$$[NaP_a] = \frac{[NaP_{total}]}{1 - 10^{(pH - pK_a)}}$$

$$M_{NaP_x} = [NaP_x] \times V \times MW_{NaP_x}$$

Minor adjustments to achieve a final pH of 8.20 were made by titrating with potassium hydroxide and 0.5M sulfuric acid.

3. *CaRGOS* Solution

With hemoglobin and NaPb solutions available, a 10% v/v sol-gel stock solution is prepared. Once all components are available, 1%wt hemoglobin is suspended in 0%, 0.5%, 1%v/v sol-gels with 0.45M NaPb, 2.5%v/v sol-gels with 0.445M NaPb, 5%v/v sol-gels with 0.25M NaPb, and 7.5% sol-gels with 0.125M NaPb by combining the necessary quantities listed in Table VIII.

TABLE VIII

RECIPE FOR HEMOGLOBIN *CARGOS* SAMPLES OF (0 – 7.5 V/V%) GEL

Component	Volume (mL) per cuvette					
	0%v/v	0.5%v/v	1%v/v	2.5%v/v	5%v/v	7.5%v/v
1%wt Hemoglobin	0.03	0.03	0.03	0.03	0.03	0.03
0.5M NaPb	2.67	2.67	2.67	2.22	1.47	0.72
10%v/v Sol-Gel	0	0.15	0.30	0.75	1.50	2.25
NFW	0.30	0.15	0.00	0.00	0.00	0.00
Total Volume	**3.00**	**3.00**	**3.00**	**3.00**	**3.00**	**3.00**

B. Experimental Procedure

1. Time and Temperature Study.

To assess integrity of hemoglobin within the samples over time, UV-vis spectroscopy was run on 2 cuvettes of each sample immediately after preparation, and 3, 6, 10, 13, 17, 20, 24, 27 and 31 days since initially stored at room temperature. Quantification of hemoglobin preservation was assessed by relative peak intensity of the 406 nm band, characteristic of the prosthetic heme group ($C_{34}H_{32}O_4N_4Fe$).

2. *CaRGOS* Size and Stability With Hemoglobin

The zeta potential and hydrodynamic size was measured for both *CaRGOS* (0.0, 0.5, & 1.0 % v/v TMOS; 0.5 M NaPb, pH 8.2; 3.0 mL) and *CaRGOS*-hemoglobin (0.0, 0.5, & 1.0 % v/v TMOS; 0.01 wt./v % Hemoglobin; 0.5 M NaPb, pH 8.2; 3.0 mL) dispersions using a NanoBrook Zeta PALS Zeta Potential Analyzer. The voltage of 3.0 V and frequency of 20.0 Hz was optimized to analyze stability of *CaRGOS* in high salt environment. The zeta potential and size were reported as an average and standard deviation of 10 readings per sample

3. Recovery of Hemoglobin

The UV-Vis spectra of stored *CaRGOS*-hemoglobin (0.0 - 7.5 % v/v TMOS; 0.01 wt./v % Hemoglobin; 0.5 M NaPb, pH 8.2; 3.0 mL) solutions were recorded on 0, 1,14, 24 and 31days to validate integrity of hemoglobin in the *CaRGOS* formulations. Polyethylene glycol (65.0 μM, 1.0 mL) was transferred to *CaRGOS*-hemoglobin samples (1.0- 7.5 % v/v TMOS; 0.01 wt./v % Hemoglobin; 0.5 M NaPb, pH 8.2; 3.0 mL) for facile re-dissolution of the silica-dispersions and another set of UV-Vis spectra were recorded.

IV. Results and Discussion of Results

A. Room Temperature Preservation

UV-Vis spectroscopy is a rapid method to validate reproducibility and stability of hemoglobin in the various *CaRGOS* formulations (0.0 – 7.5 % v/v) at room-temperature via 406 nm band representative of the heme group as well as to detect the presence of nuclease via 260 nm bump, shoulder or band arising from environmental contamination in the *CaRGOS* formulations. As shown in the Figure 14, a sharp 406 nm UV-Vis band characteristic of the prosthetic heme group was observed with hemoglobin solutions and decreases as denaturation of the native structure occurs.
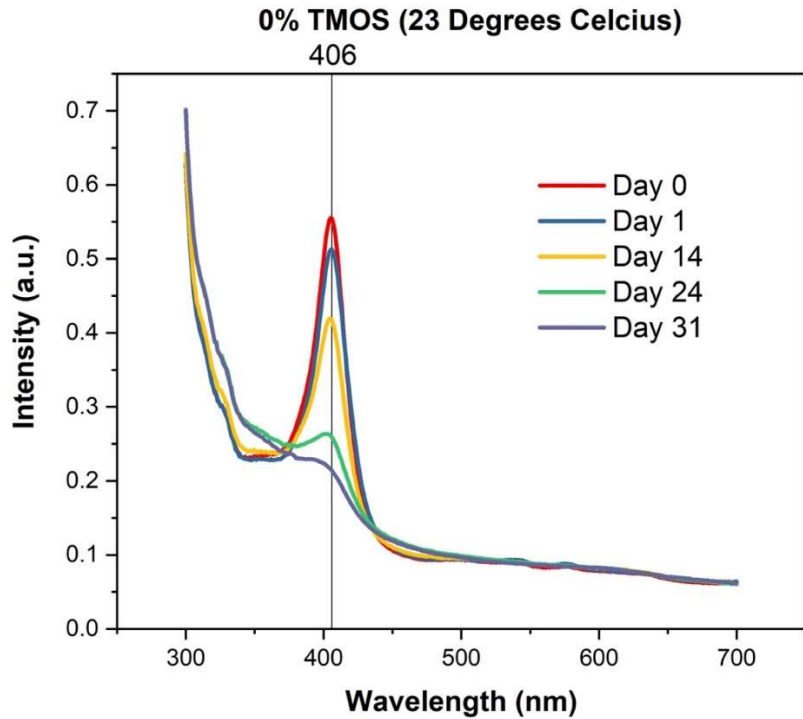

FIGURE 14 – UV-Vis Spectrum of Hemoglobin Degrading in Room Temperature Storage Over Time

While keeping hemoglobin concentration and buffer environment fixed, the *CaRGOS* concentration was varied to observe the long-term (~31 days) room-temperature stability of hemoglobin. An unaltered 406 nm UV-Vis absorbance band was observed over 31 days in high gel concentration *CaRGOS* (5.0 & 7.5 % v/v) solutions, inferring a thermally stable hemoglobin. However, a significant decrease in UV-Vis absorbance of heme group was observed with rest of the *CaRGOS* formulations (0.0 -2.5 % v/v), demonstrating a *CaRGOS*-concentration dependent trend in determining the physical and chemical stability of hemoglobin dispersions.

A control group of hemoglobin solutions without *CaRGOS* stored at room-temperature had demonstrated a significant decrease in UV-Vis absorbances: ~ 10 % in 1-week, ~ 20 % in 3- weeks and ~ 63 % in four weeks respectively. Notably, the complete denaturation of hemoglobin was not observed over 4-weeks. This inherently robust-stability of hemoglobin solutions is also facilitated by the non-contaminated buffer solutions and a careful downstream analysis. In contrast to ~ 63 % denaturation of hemoglobin control over 4 weeks, a differential response was observed in presence of *CaRGOS* formulations. Hemoglobin stability increases with each increment in *CaRGOS* concentration within the experimental range.

Relative to the control-group hemoglobin solutions, a two-fold and three-fold increase in hemoglobin stability was observed within 1.0 % v/v and 2.5 % v/v *CaRGOS* respectively as seen in Figure 15.
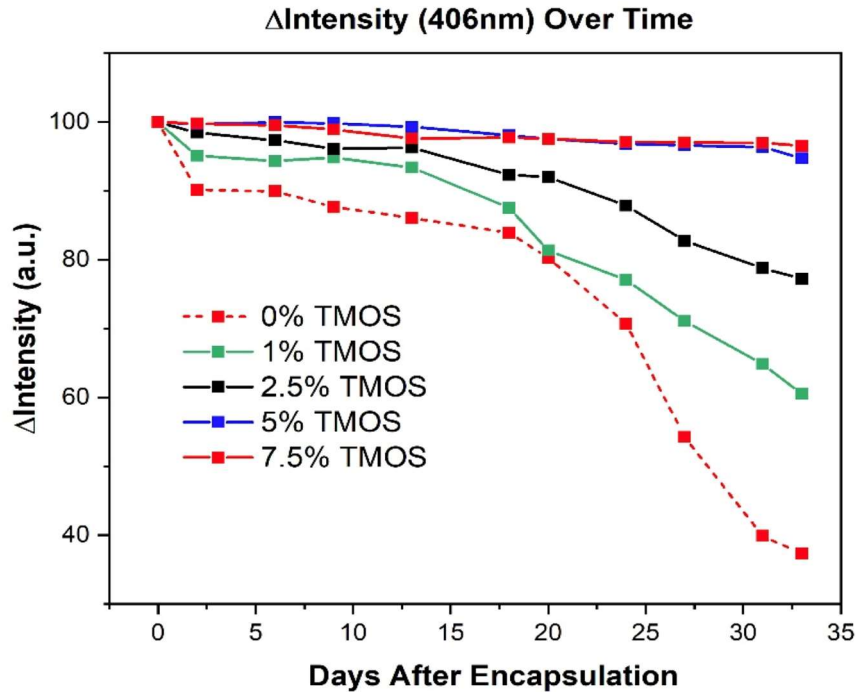
FIGURE 15 – Measured Change in Hemoglobin Peak Intensity in *CaRGOS*

Notably, all *CaRGOS* formulations had demonstrated significant hemoglobin stability up to 3-weeks storage at ambient temperature, with a small 0.0 -12.0 % degradation in the total hemoglobin content of the stored *CaRGOS* formulations. However, the high gel *CaRGOS* (5.0 and 7.5 % v/v) solutions had demonstrated nearly 100 % hemoglobin-stability up to 3-weeks and 94 % stability in 31 days under room-temperature and mechanical-handling (i.e., mixing, vortexing) based storage conditions.

An incremental stability of hemoglobin dispersions in *CaRGOS* formulations is attributed to the inherently dual-capabilities of silica formulations. As previously mentioned, silica formulations have been known to stabilize biospecimens by (a) immobilizing their native conformation in their matrices and by (b) circumventing nucleolytic and proteolytic hydrolysis of biomacromolecule's backbone, via non-covalent interaction (i.e., electrostatic, van der waals) that induce unfolding of nuclease or

protease. The 1.0 % v/v *CaRGOS* formulations are highly aqueous and contains an insignificant amount of silica content to immobilize the hemoglobin. Nevertheless, a two-fold increment in hemoglobin stability was still observed in this formula against the control hemoglobin solutions. This unique stabilization of hemoglobin is attributed to the nuclease or protease inhibiting capabilities of these silica formulations. The large-sized nanostructures (nm) with limited curvature, large surface of contact and high surface potential silica nanostructures (i.e., solid core, mesoporous) in low-salt buffer solutions had been known to unfold nuclease and avert protease activity.

B. *CaRGOS* Size and Stability with Hemoglobin

The hydrodynamic size (nm) and Zeta potential (mV) measurements were performed on the stored *CaRGOS* solutions, with and w/o hemoglobin on 0, 7 and 14 days, shown in Table IX.

TABLE IX

SIZE AND STABILITY OF HEMOGLOBIN *CARGOS* SUSPENSIONS OVER TIME

CaRGOS Concentration(v/v) %	DLS (nm)			PDI			Zeta Potential (mV)	
	Day 0	Day 7	Day 14	Day 0	Day 7	Day 14	Day 7	Day 14
0	1388 ± 624.8	233.10 ± 203.60	-	1.000 ± 0.000	0.501 ± 0.281	-	7.52 ± 13.35	-2.66 ± 1.11
0 (*with Hemoglobin*)	817.9 ± 85.75	1616.00 ± 804.20	668.7 ± 194.1	0.764 ± 0.060	1.000 ± 0.000	0.919 ± 0.095	-1.77 ± 3.79	6.39 ± 15.17
0.5	933.0 ± 29.39	648.20 ± 56.12	437.6 ± 125.3	1.000 ± 0.000	1.000 ± 0.000	0.949 ± 0.047	-6.30 ± 1.35	-18.75 ± 7.84
0.5 (*with Hemoglobin*)	830.0 ± 53.83	714.5 ± 495.9	297.8 ± 45.70	0.984 ± 0.027	0.910 ± 0.155	1.000 ± 0.000	-7.57 ± 3.50	-19.55 ± 7.49
1.0	232.2 ± 45.38	4302 ± 2590	313.4 ± 119.6	0.983 ± 0.030	0.753 ± 0.427	0.909 ± 0.158	-6.06 ± 1.60	-19.63 ± 9.99
1.0 (*with Hemoglobin*)	423.8 ± 120.8	1317 ± 313.2	364.6 ± 133.8	1.000 ± 0.000	0.351 ± 0.180	0.971 ± 0.050	14.45 ± 18.66	-9.30 ± 0.92

The colloidal dispersions of 0.0, 0.5, and 1.0 % v/v *CaRGOS* with and without hemoglobin had displayed the hydrodynamic sizes in 200- 2000 nm range and a PDI ~ 1.0, indicating highly-polydisperse and large hydrodynamic-sized nanostructures. The similar hydrodynamic sizes of *CaRGOS* formulations, with and without hemoglobin is tentatively attributed to a unique shape-recognition feature of silica nanostructures. These porous silica nanostructures may deposit congruently to the hemoglobin native conformation and match the protein shape and size, resulting in similar hydrodynamic sizes and PDI values.

A zeta potential in a – 25.0 mV to + 25.0 mV range was observed for *CaRGOS* formulations with and w/o hemoglobin, indicating instability of *CaRGOS* matrices in phosphate buffer dispersions. However, zeta potential of -(6.0 – 25.0) mV was observed with 0.5 % v/v *CaRGOS* formulations, with and without hemoglobin, which displayed fair stability and resistance to aggregation in NaPb dispersions. The superior stability of 0.5 % v/v *CaRGOS* formulations over the rest of the *CaRGOS* formulations is due to finely dispersing *CaRGOS* nanostructures in comparison to highly viscous and sedimenting silica matrices in NaPb dispersions, respectively.

C. Hemoglobin Recovery.

A quick re-dissolution of more viscous *CaRGOS*-hemoglobin formulations was observed upon addition of polyethylene glycol or PEG (65μM, 2KDa). Figure 16 shows a three to five-fold increase in hemoglobin's UV-Vis absorbance (406 nm) in the *CaRGOS* formulations upon PEGylation.
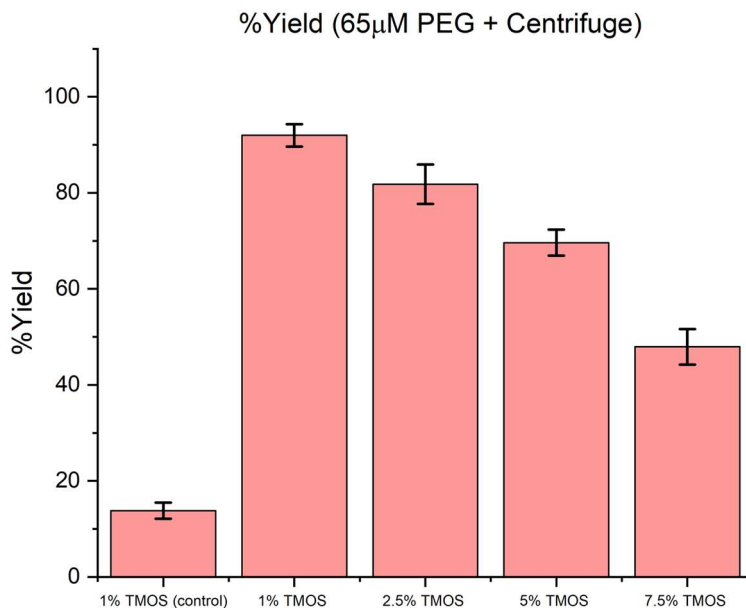
FIGURE 16 – Percent Yield of Recoverable Hemoglobin from *CaRGOS* Matrix

This large increment in the absorbance intensity of heme group is attributed to a synergistic hydrophilicity imparted by PEG to the *CaRGOS* silica formation, allowing a facile passage and release of hemoglobin from the *CaRGOS* matrices without any loss of protein nativity. As previously mentioned, an ideal ensilication matrix allows efficient bioanalyte immobilization (i.e., encapsulation entrapment or collaterally depositing) and a facile passage without any physical rupture. Therefore, the highly porous and moderately viscous *CaRGOS* formulations require PEGylation for protein-retrieval after long-term storage.

V. CONCLUSIONS

CaRGOS was synthesized by a standard microwave method and hemoglobin protein was stored in it under slightly basic buffer conditions. UV-Vis, DLS, and zeta potential measurements were performed to analyze hemoglobin's thermal and mechanical (i.e., mixing, vortexing) stability over 31 days. Silica nanomatrices stabilizes biospecimens by immobilization of biospecimens and inhibition of environmental contamination (i.e., nuclease and protease). This is particularly evident based on the UV-Vis analysis of high concentration *CaRGOS* (5.0 & 7.5) v/v % formulations, which displayed excellent stability of hemoglobin protein over 31 days. At low concentration *CaRGOS* (1.0 v/v%) formulations with tiny silica content, the hemoglobin solutions are fairly stable based on UV-Vis analysis, deciphering a strong correlation between hemoglobin stability and nuclease or protease averting capability of silica matrices. DLS studies confirmed a highly polydisperse nanostructure framework of *CaRGOS* formulations and zeta potential studies shows that only intermediate *CaRGOS* (0.5 v/v %) concentrations are stable in phosphate buffer dispersions. The robust storage and transport are the promise of this innovation. Thermal stability studies with other proteins are currently underway.

VI. RECOMMENDATIONS

Though the application of *CaRGOS* has been proven viable with miRNA storage and preservation, there are still more ways sol-gel solutions can be tuned to assist in biomolecular and pharmaceutical endeavors. With the simplicity of the *CaRGOS* manufacturing process it could easily be incorporated into a microfluidics system. Lab on a chip research could also be improved by incorporating *CaRGOS* as a stabilizing agent for proteins and other unstable macromolecules.

Molecular dynamics simulations would also be a direction that future studies of *CaRGOS* could branch into. With computational chemistry and known properties of many biomolecules already available, ideal solution conditions for *CaRGOS* applications for many other biomolecules could be derived mathematically and then tested experimentally rather than the other way around.

With *CaRGOS* formulation proving to have potential application in cancer immunotherapy and MDR studies by conjugating doxorubicin to *CaRGOS* and RNA architectures, studies should be conducted with living subjects to test its feasibility in practice.
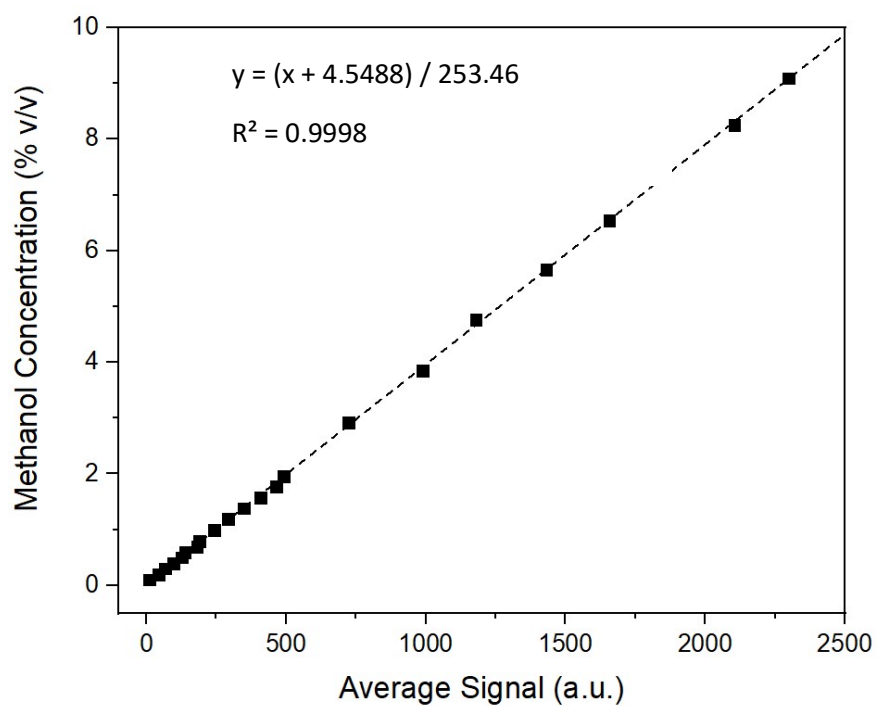
FIGURE 17 – Raman Peak Intensity Vs. Methanol Volume Percent Calibration Curve
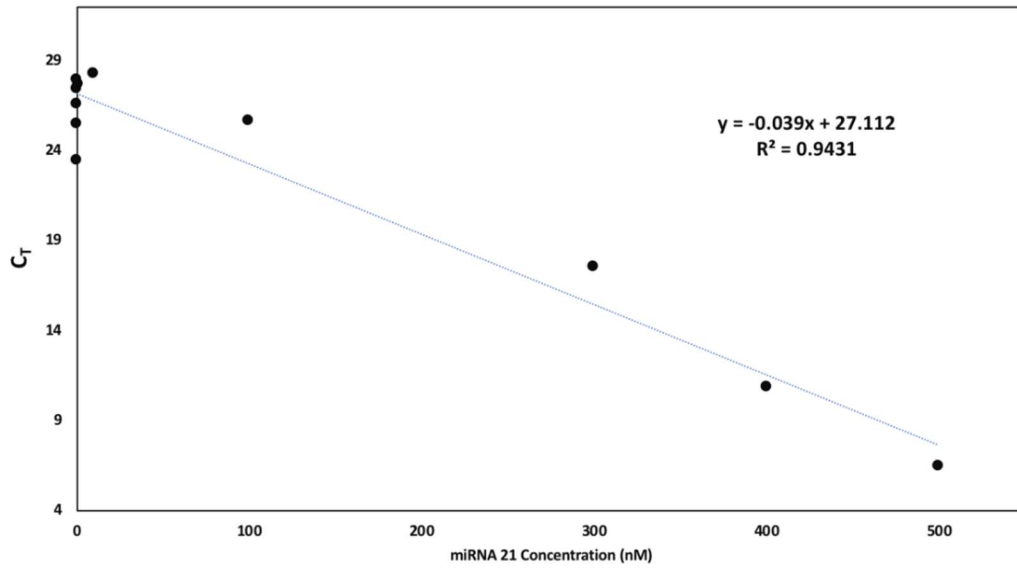
FIGURE 18 – Critical Threshold Vs. miRNA 21 Concentration: 0.5 % v/v *CaRGOS* Solution Calibration Curve

$$y = -0.039x + 27.112$$
$$R^2 = 0.9431$$
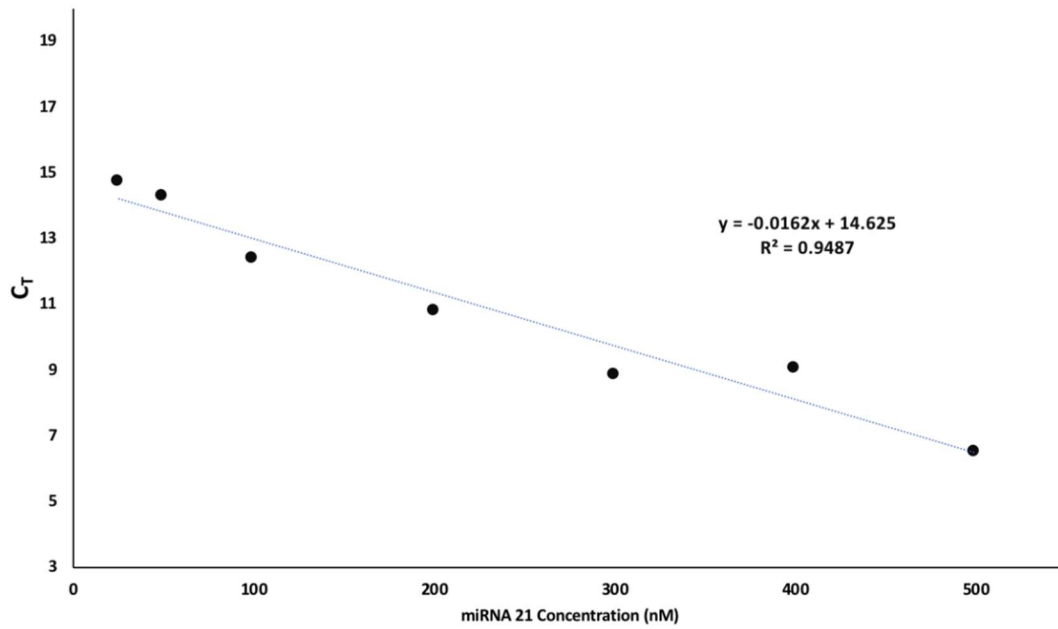
FIGURE 19 – Critical Threshold Vs. miRNA 21 Concentration Calibration Curve for Salinity Study

$$y = -0.0162x + 14.625$$
$$R^2 = 0.9487$$
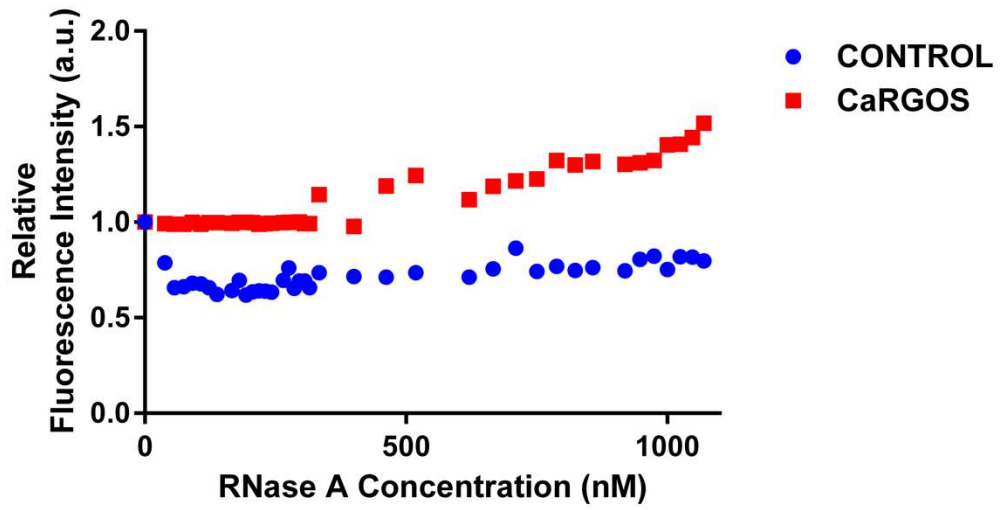
FIGURE 20 – Relative Fluorescence Intensity of Ethidium Bromide Vs. RNase A

Concentration Range 0-1200nM

$$Y=8426.1X + 423.15$$
$$R^2= 0.9982$$

FIGURE 21 – Fluorescence Vs. DOX Concentration Calibration Curve

REFERENCES

1. Lou, J.J., et al., *A review of room temperature storage of biospecimen tissue and nucleic acids for anatomic pathology laboratories and biorepositories.* Clin Biochem, 2014. **47**(4-5): p. 267-73.

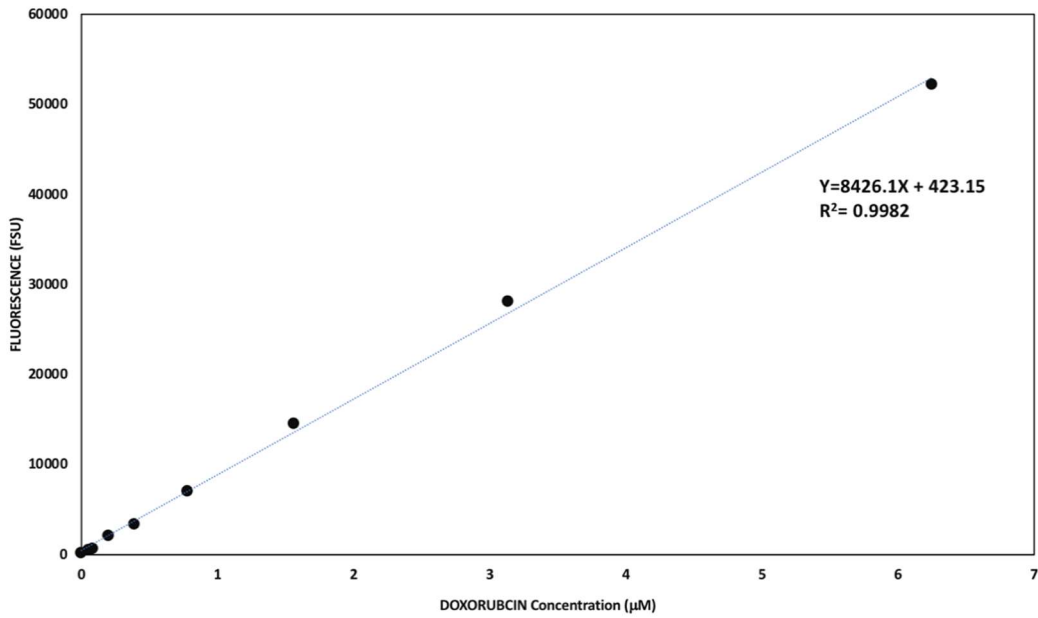2. Fabre, A.L., et al., *An efficient method for long-term room temperature storage of RNA.* Eur J Hum Genet, 2014. **22**(3): p. 379-85.

3. Mutter, G.L., et al., *Comparison of frozen and RNALater solid tissue storage methods for use in RNA expression microarrays.* BMC Genomics, 2004. **5**: p. 88.

4. Ibberson, D., et al., *RNA degradation compromises the reliability of microRNA expression profiling.* BMC Biotechnol, 2009. **9**: p. 102.

5. Riegman, P.H., et al., *Biobanking for better healthcare.* Mol Oncol, 2008. **2**(3): p. 213-22.

6. Wang, Z., et al., *Circulating microRNA-21 as noninvasive predictive biomarker for response in cancer immunotherapy.* Med Hypotheses, 2013. **81**(1): p. 41-3.

7. Akers, J.C., et al., *Optimizing preservation of extracellular vesicular miRNAs derived from clinical cerebrospinal fluid.* Cancer Biomark, 2016. **17**(2): p. 125-32.

8. Zhu, J., et al., *MiR-20b, -21, and -130b inhibit PTEN expression resulting in B7-H1 over-expression in advanced colorectal cancer.* Hum Immunol, 2014. **75**(4): p. 348-53.

9. Gupta, R. and N.K. Chaudhury, *Entrapment of biomolecules in sol-gel matrix for applications in biosensors: problems and future prospects.* Biosens Bioelectron, 2007. **22**(11): p. 2387-99.

10. Mackenzie, J.D.B., E. P., *Physical Properties of Sol-Gel Coatings.* Journal of Sol-Gel Science and Technology, 2000. **1**(19): p. 6.

11. Braun, S.R., S.; Zusman, R.; Avnir, D.; Ottolenghi, M., *Biochemically active sol-gel glasses: The trapping of enzymes.* Material Letters, 2007. **14**(61): p. 3.

12. Díaz-García, M.E. and R.B. Laínño, *Molecular Imprinting in Sol-Gel Materials: Recent Developments and Applications.* Microchimica Acta, 2005. **149**(1): p. 19-36.

13. Ellerby, L., et al., *Encapsulation of proteins in transparent porous silicate glasses prepared by the sol-gel method.* Science, 1992. **255**(5048): p. 1113-1115.

14. Ratner, B.D. and S.J. Bryant, *Biomaterials: where we have been and where we are going.* Annu. Rev. Biomed. Eng., 2004. **6**: p. 41-75.

15. Hench, L.L. and J.M. Polak, *Third-generation biomedical materials.* Science, 2002. **295**(5557): p. 1014-1017.

16. Roach, P., et al., *Modern biomaterials: a review—bulk properties and implications of surface modifications.* Journal of Materials Science: Materials in Medicine, 2007. **18**(7): p. 1263-1277.

17. Liu, X., et al., *Evaluation of DNA/RNAshells for room temperature nucleic acids storage.* Biopreserv Biobank, 2015. **13**(1): p. 49-55.

18. Crowe, J.H., J.F. Carpenter, and L.M. Crowe, *The role of vitrification in anhydrobiosis.* Annu Rev Physiol, 1998. **60**: p. 73-103.

19. Chen, Z.H., S.; Shi, M.; Liu, G.; Chen, Z.; Chang, J.; Wu, C.; Xiao, Y., *Immunomodulatory effects of mesoporous silica nanoparticles on osteogenesis: From nanoimmunotoxicity to nanoimmunotherapy.* Applied Materials Today, 2018. **10**: p. 9.

20. Meng, H., et al., *Engineered design of mesoporous silica nanoparticles to deliver doxorubicin and P-glycoprotein siRNA to overcome drug resistance in a cancer cell line.* ACS Nano, 2010. **4**(8): p. 4539-50.

21. Schlipf, D.M., S.E. Rankin, and B.L. Knutson, *Pore-size dependent protein adsorption and protection from proteolytic hydrolysis in tailored mesoporous silica particles.* ACS Appl Mater Interfaces, 2013. **5**(20): p. 10111-7.

22. Shen, J., et al., *Mesoporous silica nanoparticles loading doxorubicin reverse multidrug resistance: performance and mechanism.* Nanoscale, 2011. **3**(10): p. 4314-22.

23. Peng, S., et al., *Metal-organic frameworks for precise inclusion of single-stranded DNA and transfection in immune cells.* Nat Commun, 2018. **9**(1): p. 1293.

24. Shang, W., et al., *Unfolding of ribonuclease A on silica nanoparticle surfaces.* Nano Lett, 2007. **7**(7): p. 1991-5.

25. Vertegel, A.A., R.W. Siegel, and J.S. Dordick, *Silica nanoparticle size influences the structure and enzymatic activity of adsorbed lysozyme.* Langmuir, 2004. **20**(16): p. 6800-7.

26.   Cha, B.G., J.H. Jeong, and J. Kim, *Extra-Large Pore Mesoporous Silica Nanoparticles Enabling Co-Delivery of High Amounts of Protein Antigen and Toll-like Receptor 9 Agonist for Enhanced Cancer Vaccine Efficacy.* ACS Cent Sci, 2018. **4**(4): p. 484-492.

27.   Chen, Y.C., et al., *Thermal stability, storage and release of proteins with tailored fit in silica.* Sci Rep, 2017. **7**: p. 46568.

28.   Perumal, S., S. Ramadass, and B. Madhan, *Sol-gel processed mupirocin silica microspheres loaded collagen scaffold: a synergistic bio-composite for wound healing.* Eur J Pharm Sci, 2014. **52**: p. 26-33.

29.   Gupta, G., et al., *CVD for the facile synthesis of hybrid nanobiomaterials integrating functional supramolecular assemblies.* Langmuir, 2009. **25**(23): p. 13322-7.

30.   Van Blaaderen, A. and A. Vrij, *Synthesis and Characterization of Colloidal Dispersions of Fluorescent, Monodisperse Silica Spheres.* LANGMUIR, 1992. **8**(12): p. 2921.

31.   Cusanovich, M.A., *The Chemistry of Silica (Iler, Ralph K.).* Journal of Chemical Education, 1980. **57**(11): p. A324.

32.   Issa, A.A. and A.S. Luyt, *Kinetics of Alkoxysilanes and Organoalkoxysilanes Polymerization: A Review.* Polymers (Basel), 2019. **11**(3).

33.   Brinker, C.J. and G.W. Scherer, *Sol-gel science : the physics and chemistry of sol-gel processing.* 1990, Boston: Academic Press. xiv, 908 p.

34.   Livage, J. and C. Sanchez, *Sol-gel chemistry.* Journal of Non-Crystalline Solids, 1992. **145**: p. 11-19.

35.   Zerda, T.W., I. Artaki, and J. Jonas, *Study of polymerization processes in acid and base catalyzed silica sol-gels.* Journal of Non-Crystalline Solids, 1986. **81**(3): p. 365-379.

36.   Mammone, J., S. Sharma, and M. Nicol, *Raman spectra of methanol and ethanol at pressures up to 100 kbar.* The Journal of Physical Chemistry, 1980. **84**(23): p. 3130-3134.

37.   González, P., et al., *Raman spectroscopic study of bioactive silica based glasses.* Journal of non-crystalline solids, 2003. **320**(1-3): p. 92-99.

38.   Bergna, H.E., *The colloid chemistry of silica*. 1994: ACS Publications.

39.   Anedda, A., et al., *Surface hydroxyls in porous silica: a Raman spectroscopy study.* Materials Science and Engineering: C, 2003. **23**(6-8): p. 1069-1072.

40.   Serra, J., et al., *FTIR and XPS studies of bioactive silica based glasses.* Journal of Non-Crystalline Solids, 2003. **332**(1-3): p. 20-27.

41. Glock, K., et al., *Novel opportunities for studying the short and medium range order of glasses by MAS NMR, 29Si double quantum NMR and IR spectroscopies.* Journal of Non-Crystalline Solids, 1998. **232-234**: p. 113-118.

42. Young, S.K., *Organic-inorganic composite materials: Molecular tailoring of structure-property relationships.* 1999.

43. Hanaor, D., et al., *The effects of carboxylic acids on the aqueous dispersion and electrophoretic deposition of ZrO2.* Journal of the European Ceramic Society, 2012. **32**(1): p. 235-244.

44. Larsson, M., A. Hill, and J. Duffy, *Suspension stability; why particle size, zeta potential and rheology are important.* Ann. Trans. Nordic Rheol. Soc, 2012. **20**: p. 209-214.

45. Salopek, B., D. Krasic, and S. Filipovic, *Measurement and application of zeta-potential.* Rudarsko-geolosko-naftni zbornik, 1992. **4**(1): p. 147.

46. Ostolska, I. and M. Wiśniewska, *Application of the zeta potential measurements to explanation of colloidal Cr2O3 stability mechanism in the presence of the ionic polyamino acids.* Colloid and Polymer Science, 2014. **292**(10): p. 2453-2464.

47. Harrill, A.H., et al., *MicroRNA Biomarkers of Toxicity in Biological Matrices.* Toxicol Sci, 2016. **152**(2): p. 264-72.

48. Lan, H., et al., *MicroRNAs as potential biomarkers in cancer: opportunities and challenges.* Biomed Res Int, 2015. **2015**: p. 125094.

49. Xiaolin, W.N.B., A.; Gisela, S. A.; Maria, V. T.; Christophe, H.; Martin, F. D.; Thibaud, C., *Sol-gel Encapsulation of Biomolecules and Cells for Medicinal Applications.* Current Topics in Medicinal Chemistry, 2015: p. 21.

50. Lee, C.J., J.H. Jung, and T.S. Seo, *3D porous sol-gel matrix incorporated microdevice for effective large volume cell sample pretreatment.* Anal Chem, 2012. **84**(11): p. 4928-34.

51. Kandimalla, V.B.T., V. S.; Ju, H., *Immobilization of Biomolecules in Sol–Gels: Biological and Analytical Applications.* Critical Reviews in Analytical Chemistry, 2006. **2**(36): p. 33.

52. To, K.K., *MicroRNA: a prognostic biomarker and a possible druggable target for circumventing multidrug resistance in cancer chemotherapy.* J Biomed Sci, 2013. **20**: p. 99.

53. Zhu, Q., et al., *Extracellular control of intracellular drug release for enhanced safety of anti-cancer chemotherapy.* Sci Rep, 2016. **6**: p. 28596.

54. Larsericsdotter, H., S. Oscarsson, and J. Buijs, *Thermodynamic Analysis of Proteins Adsorbed on Silica Particles: Electrostatic Effects.* J Colloid Interface Sci, 2001. **237**(1): p. 98-103.

55. Hui, C.Y.L., P. S.; , *Investigation of RNA structure-switching aptamers in tunable sol–gel-derived materials.* Journal of Sol-Gel Science and Technology, 2019. **89**(1): p. 9.

56. Mulyasasmita, W., J.S. Lee, and S.C. Heilshorn, *Molecular-level engineering of protein physical hydrogels for predictive sol-gel phase behavior.* Biomacromolecules, 2011. **12**(10): p. 3406-11.

57. Carrasquilla, C., et al., *Stabilizing structure-switching signaling RNA aptamers by entrapment in sol-gel derived materials for solid-phase assays.* J Am Chem Soc, 2012. **134**(26): p. 10998-1005.

58. Lum, R.M., L.M. Wiley, and A.I. Barakat, *Influence of different forms of fluid shear stress on vascular endothelial TGF-beta1 mRNA expression.* Int J Mol Med, 2000. **5**(6): p. 635-41.

59. Piskorz, A.M., et al., *Methanol-based fixation is superior to buffered formalin for next-generation sequencing of DNA from clinical cancer samples.* Ann Oncol, 2016. **27**(3): p. 532-9.

60. Lee, C.S. and G. Belfort, *Changing activity of ribonuclease A during adsorption: a molecular explanation.* Proc Natl Acad Sci U S A, 1989. **86**(21): p. 8392-6.

61. Santoro, J., et al., *High-resolution three-dimensional structure of ribonuclease A in solution by nuclear magnetic resonance spectroscopy.* J Mol Biol, 1993. **229**(3): p. 722-34.

62. Roach, P., D. Farrar, and C.C. Perry, *Surface tailoring for controlled protein adsorption: effect of topography at the nanometer scale and chemistry.* J Am Chem Soc, 2006. **128**(12): p. 3939-45.

63. Wang, X., et al., *Comprehensive Mechanism Analysis of Mesoporous-Silica-Nanoparticle-Induced Cancer Immunotherapy.* Adv Healthc Mater, 2016. **5**(10): p. 1169-76.

64. Tripathy, D.R., A.K. Dinda, and S. Dasgupta, *A simple assay for the ribonuclease activity of ribonucleases in the presence of ethidium bromide.* Anal Biochem, 2013. **437**(2): p. 126-9.

65. Rubio, A.R.B., N.; Leal, J. M.; Garcia, B., *Doxorubicin binds to duplex RNA with higher affinity than ctDNA and favours the isothermal denaturation of triplex RNA.* RSC Advances, 2016. **6**(103): p. 10.

66. Brown, J.S., R. Sundar, and J. Lopez, *Combining DNA damaging therapeutics with immunotherapy: more haste, less speed.* Br J Cancer, 2018. **118**(3): p. 312-324.

67. Jin, H.Y., et al., *Transfection of microRNA Mimics Should Be Used with Caution.* Front Genet, 2015. **6**: p. 340.

68.   Raynal, B., et al., *Quality assessment and optimization of purified protein samples: why and how?* Microb Cell Fact, 2014. **13**: p. 180.